Optimisation of Downskin Parameters to produce Metallic Parts Via Laser Powder Bed Fusion process: an overview

The International Journal of Advanced Manufacturing Technology (2022) 123:2159–2182
https://doi.org/10.1007/s00170-022-10314-z

CRITICAL REVIEW

Optimisation of downskin parameters to produce metallic parts via laser powder bed fusion process: an overview

Vittorio Viale[1] · John Stavridis[1,2] · Alessandro Salmi[2] · Federica Bondioli[3] · Abdollah Saboori[2]

Received: 5 May 2022 / Accepted: 11 October 2022 / Published online: 2 November 2022

Abstract
Additive manufacturing technologies are considered advanced processes in which it is possible to produce complex shape components layer-by-layer. In these technologies, it is reported that in producing parts with angles higher than 45°, no support is required. Depending on the material below this angle, it is necessary to use the support structures to dissipate the heat and counterbalance the force of the recoding blade. During the building process, it is well documented that there is a risk of part detachment at low angles that can result in failure. On the other hand, a heavy dross formation on the downskin surface will occur if no failure happens, resulting in a surface with scarce quality. Hence, many efforts have been undertaken to face this challenge and study the effect of various parameters, such as layer thickness, laser power, and scan speed, on the quality of the downskin surface of the minimum printable angle without the support requirement. This review offers an overview of the last progress on the effect of process parameters on the surface quality of the downward surfaces in the production of complex parts via the laser powder bed fusion process. This review highlights the best practices that may be considered for future works to find effective parameters for producing complex shape components with low angles without support structures.

Keywords Additive manufacturing · Laser powder bed fusion · Downskin parameters · Support structure

1 Introduction

Additive manufacturing (AM) is a name that represents all the technologies that create 3D objects by adding layer upon layer of the material [1, 2]. The key concept is the additive process, opposite to the most common subtracting ones (i.e. machining), a revolutionary kind of manufacturing for which the final piece will be made by adding material layer by layer, causing of reduction in the waste of materials [3–5]. Moreover, using AM technologies, no specific tools are required to produce the components and complex shape parts are built directly from the feedstock material using an AM machine [6, 7].

Over the last years, in comparison to the 3D printing of polymers, metal AM could attract lots of attention, mainly owing to the improvements in the machinery, lasers and powder production processes that resulted in the achievement of high-quality parts [8, 9]. In general, AM systems are classified according to their heat source (laser, electron beam and plasma arc), the type of feedstock (wire or powder), how the feedstock is delivered and the dimension and quality of the produced component [10–13]. The first classification introduced by ASTM is based on feedstock delivery approaches [14]. According to this classification, the two most common classes of metal AM are powder bed fusion (PBF) and directed energy deposition (DED) [15, 16]. In the PBF process, the heat source can be either laser (L-PBF) or electron beam (EB-PBF or EBM). On the other hand, in the DED process, three different heat sources, such as laser (L-DED), electron beam (EB-DED) and plasma arc (PA-DED), can be used [17, 18].

It is well documented that AM processes can reduce the number of operations needed to produce an end-usable part and transform several processes with a single-step process

✉ Abdollah Saboori
abdollah.saboori@polito.it

1 Prima Additive SpA, Via Torino Pianezza 36, 10093 Torino, Collegno, Italy

2 Integrated Additive Manufacturing Center (IAM), Department of Management and Production Engineering, Politecnico Di Torino, Corso duca Degli Abruzzi 24, 10129 Torino, Italy

3 Department of Applied Science and Technology, Politecnico Di Torino, Corso duca Degli Abruzzi 24, 10129 Torino, Italy

plus a finishing step [19, 20]. When the production of a batch of pieces by AM or with a CNC (computer numerical control) machine is compared, it is revealed that in a CNC machine, a semi-complex part can be produced after several processes and, as a consequence, result in a very long production process. In contrast, in AM, a piece can be produced just in a few hours (depending on the part dimension), while a high-quality finishing may take a few days [21, 22]. However, this should be underlined that through the AM process, it is possible to simultaneously produce more pieces in a single build in a shorter time compared to their production through the CNC machine. On the other hand, the part's complexity is a fundamental aspect of AM. Since the complex shapes are directly obtained during the building process, the cost depends on the shape and the quantity of used material. Therefore, the gain using AM increases with the complexity of parts compared to traditional manufacturing processes, where more phases are required [23, 24].

Moreover, from the design point of view, some components, such as lattice structures, undercut and internal features, are impossible to be produced using CNC machines. Instead, through the AM technologies, it would be possible to overcome the limitations of the subtractive manufacturing method and produce them in the final shape directly from the feedstock materials [25, 26]. Although AM will not replace conventional production methods, it can acquire importance in different niche areas such as aerospace, medical and dental, automotive and jewellery. AM can play a key role in aerospace, where optimal thermo-mechanical characteristics are required and in medical and dental fields, where a single piece's weight and personalisation are key factors [27, 28]. One of the new relevant aspects of AM technology is producing lattice structures that reduce weight and create new structures [29, 30]. However, the production of the components with the features mentioned above would face several challenges that should be considered in their design phase [31, 32].

One of the important aspects of design for AM that have been investigated markedly is downskin which is indicated some layers (2–5) above the supports or the powder in downward-facing surfaces (Fig. 1) [34, 35]. This importance comes back to the variation of heat conduction as a function of the relative density. It is well reported that the heat conduction for the powder is one hundred times lower than the solidly supported zones [36]. Depending on their type, the supports can dissipate the heat generated during the process, but on the other hand, the more they dissipate the heat (e.g. block support), the more difficult it would be to remove. However, it is reported that in order to obtain good mechanical properties and surface finishing of the overhanging surfaces, the use of a solid/block support is recommended to dissipate more heat, but this will also lead to an increase in the cost in terms of material, time in printing and post-processing operations [21, 37]. On the other hand, if the accumulated heat does not dissipate efficiently, the part will face issues like dross formation and warping [38, 39]. The dross formation increases roughness on the surface, causing the need for post surface treatment to achieve the desired surface quality [40]. The warping is caused by the melt pool's quick cooling that generates tensile stresses inside the layer [41]. It is well documented that if this stress is not counterbalanced by the presence of support, warpage and with its accumulation, delamination will occur [42].

From the design point of view, it is possible to define a critical angle in which, above that angle, the use of support structures is not necessary [43]. This angle is, in general, around 45° which can be altered depending on the material [44]. However, it should be noticed that it would be possible to print without support structures using optimised downskin parameters, even below this critical angle. In fact, this set of parameters generates a lower amount of heat than the process parameters normally used to print the part.

In general, several parameters can affect the downskin quality; those regarding the energy input (laser power, spot diameter and scanning speed), the ones controlling the offset between layers (tilting angle, layer thickness and hatch distance) and, finally, the parameters influencing the residual stresses (scanning length and the relationship between scanning direction and tilting angle) [45, 46].

Over the past years, optimising the downskin parameters could attract attention. For instance, Bassoli et al. tried to figure out a generalised holistic method to test parameters for all the steps in the part fabrication through the L-PBF process [47]. In another work, Covarrubias and Eshraghi found an equation to evaluate the minimum critical angle for producing superalloy components [48]. Wang et al. analysed the influence of laser speed, laser power and vector length on the quality of the oblique surfaces [45]. Minetola et al. studied the effect of the speed, power and hatch distance on the porosity, accuracy and roughness of the Hastelloy X part produced using the L-PBF process [49]. Sarkar et al. analysed the influence of the scanning strategy and the aspect ratio on the quality of the overhang surfaces in the L-PBF process [50].

It is evident that several studies have been carried out to improve the downskin quality; however, so far, no article has systematically reviewed and highlighted the importance of the downskin process parameter optimisation on the surface quality of the L-PBF components. Hence, this work aims to systematically review the current state of the art in optimising downskin parameters for the components produced via the L-PBF process. For this reason, the literature was comprehensively reviewed based on the factors that mainly affect the quality of the downskin surfaces. The effective process parameters were explained after that, considering the L-BPF process at the centre of the discussion. In this work, first,

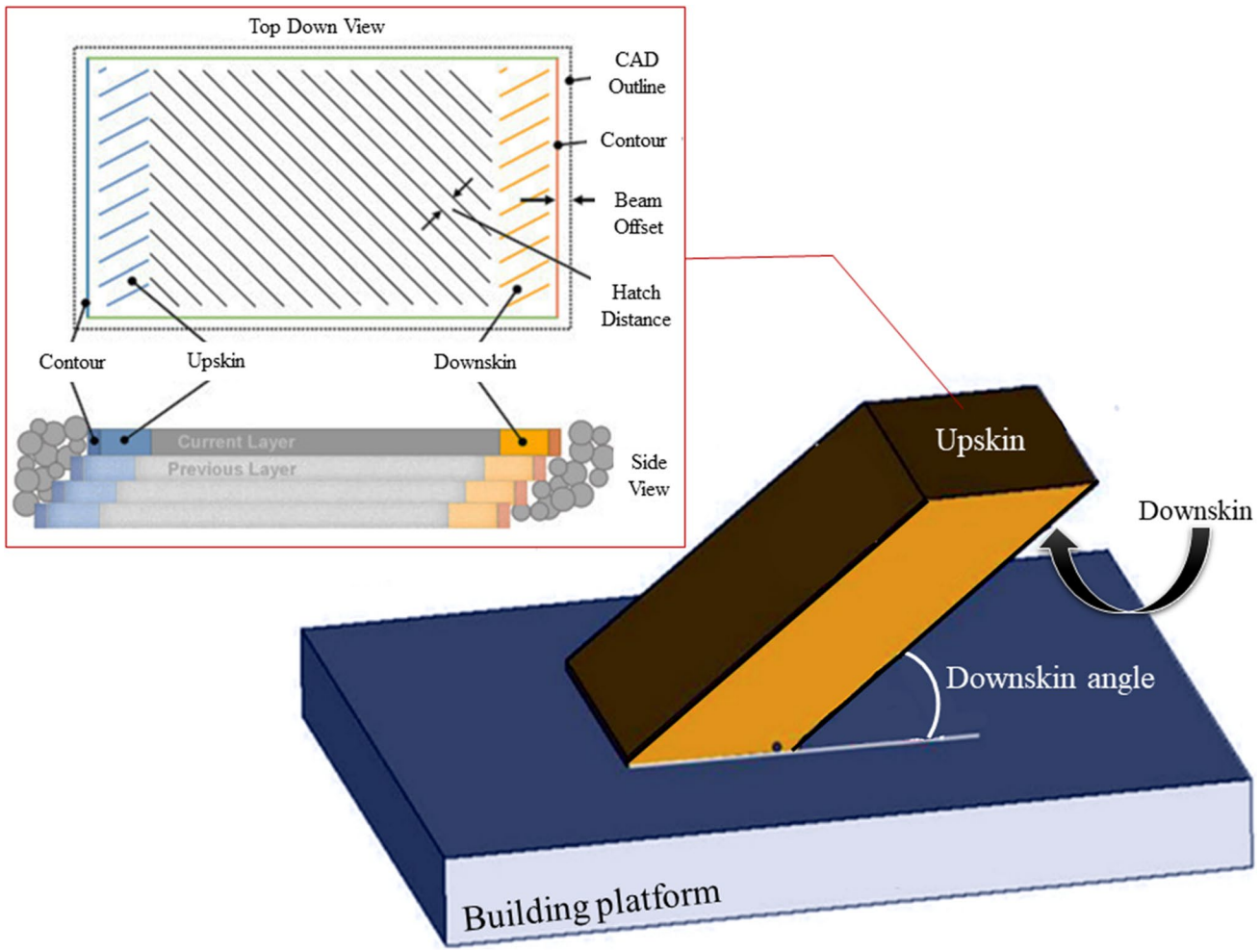

Fig. 1 Schematic of the downskin and upskin.process parameters [33]

the main powder bed fusion processes will be described and compared in detail. Thereafter, all the physical phenomena involved in the laser/powder interaction are explained. In the next section, all the downskin process parameters are introduced, and their influence is discussed in detail. In the end, future perspectives and main conclusions are drawn.

2 Powder bed fusion

2.1 Laser powder bed fusion

In the PBF processes, a high energy heat source selectively melts the powder layer according to the computer-aided design (CAD) model. Thereafter, the solidified layer moves downward for a distance equal to the layer thickness and thanks to the recoating blade, the powder is equally spread on the bed and creates a new powder layer. This sequence is repeated until the component is completely built [51, 52].

Apart from the L-PBF, several names are used to indicate the same process: direct metal laser sintering (DMLS), selective laser melting (SLM) and selective laser sintering (SLS) [53, 54]. This process can be used, for instance, to develop new titanium alloys following the in-situ alloying approach to achieve new materials with superior properties compared to the commercially available alloys [53, 55]. Other advantages of the L-PBF technology are the design freedom, the possibility to build lightweight structures (e.g. lattice structures), and the design of personalised anatomical parts [56, 57].

During the L-PBF process, a high laser power combines with a thin layer of powder to create a melt pool that will quickly solidify and result in a strong shrinkage in the material and, consequently, the stress in part [58]. Therefore, several approaches have been developed to counterbalance these stresses so as to prevent the distortions or delaminations between the layers during the building process [45]. These stress counterbalancing can be achieved by a good adhesion with the previous layers

or supports and optimised process parameters such as line offset, laser power, laser speed, and hatch distance (Fig. 2).

2.2 Electron beam powder bed fusion

Compared to the L-BPF process, EB-BPF has some advantages, such as higher productivity, being under a vacuum that makes the reactive materials processable and being a hot process that makes the brittle materials processable [54, 55]. In the EB-PBF technology, also known as EBM, an electron beam is employed as a heat source to selectively melt the powder layer following a CAD file [53, 54]. In the EB-PBF process, the electrons are emitted by a filament heated at temperatures higher than 2500 °C and then accelerated through an anode. Then, the beam is controlled using three coils before arriving in the vacuum chamber, where it melts the powder layer. EBM technology makes it possible to achieve high power (6 kW) with a narrow beam that facilitates reaching extremely high temperatures during the build process [59, 60]. The EBM process makes it possible to process refractory materials thanks to the high vacuum, allowing building parts with less impurities, giving higher strength properties to the material. Usually, the electron beam is also used for preheating the powders to sinter the powder bed, allowing the decrease of the stresses in the final piece caused by high thermal gradient and rapid solidification [10, 61].

3 Laser-powder interaction in LPBF process

One of the advantages of metal AM technologies is the approach that they can break the constraints caused by tooling [25]. The main rules are to avoid thinking of conventional design principles, capitalise on the capabilities of AM, rethink the whole assembly (freeform design and intelligent integrations), use as little raw material as possible, and design the optimal shape accordingly to functionality. However, during the PBF processes, several aspects and parameters that affect the final quality of the piece must be considered. These aspects depend on lots of factors; for example, in some cases, using the same machine and the same material with powders produced by different companies, different optimal parameters are required for their consolidation. Moreover, the presence of various forces and thermal gradients within the melt pool makes studying its behaviour very complicated and cannot be modelled easily by the software [62]. For this reason, it is very important to know at least the concepts that regulate the processes. Two factors that affect the resolution of the process are the laser profile and the powder characteristics. When the heat source impacts the powder bed, a melting pool includes several phenomena, such as Marangoni convection and evaporation [54].

Moreover, the boundaries between the melt pool and the powder can potentially permeate the liquid phase into the powder. This effect is enhanced by the dynamic evolution of the melting pool. It is also interesting how the heat source interacts with the powder. Both the laser and the electron beam have a beam characterised by a Gaussian distribution

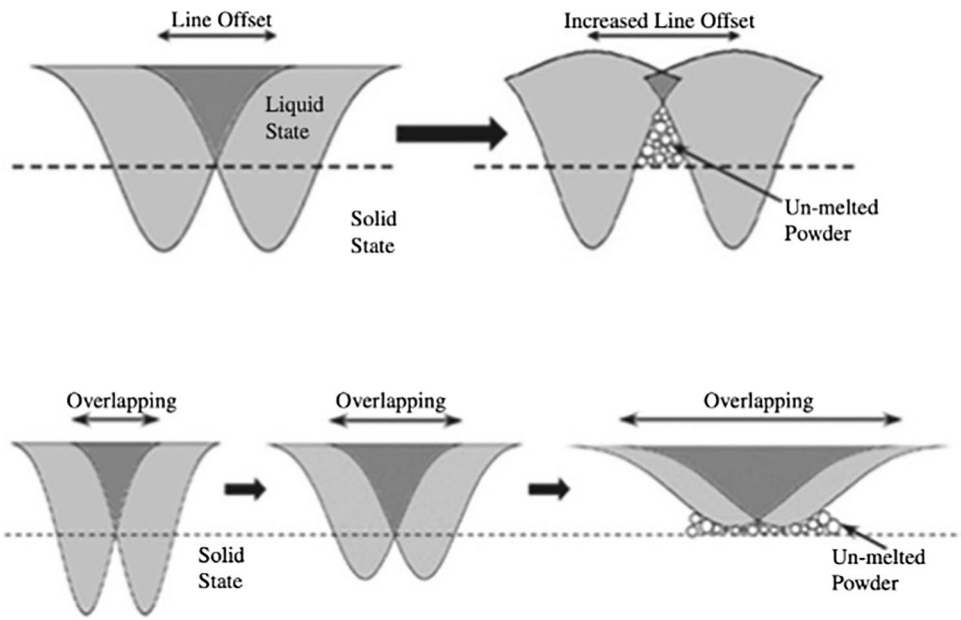

Fig. 2 Representative of the melt pool formation during the LPBF process [10]

with maximum intensity in the centre of the beam and a radial decrease. The intensity can be evaluated as [45]:

$$I(r,\omega) = I_0 \exp\left(-\frac{2r^2}{w^2}\right) \quad (1)$$

where I is the energy intensity, I_0 is the maximum intensity at the beam centre, r is the radial distance from the beam centre, and ω is the characteristics of beam width until the Gaussian distribution is 1% of the peak intensity. When the laser impacts the powder, the particles absorb a part of its energy, and the remaining one is reflected. However, the reflection can escape from the bed, go between the particles, and be completely absorbed. For this reason, the absorption rate of a powder is generally higher than the absorption of its solid one, which has a higher reflection. Nonetheless, it is also complicated to generalise a specific absorption value for a powder since its morphology, size distribution, and surface quality depend on several factors that can be different for the same material produced using different powder production methods. In fact, each powder that includes fine and coarse particles has a Gaussian particle size distribution (PSD). It is well documented that the PSD of each powder is a very important characteristic that significantly affects its flowability, the packing density of the powder bed and its melting and consolidation (Fig. 3) [10]. As regards the powder spreading mechanism in different systems, various mechanisms such as rollers, comb blades, sweep blades and moving hoppers have been developed so far. The roller is characterised by a better powder bed packing density, but it also causes compressive and shear stresses that can have negative effects. While blade spreading systems generally generate less stress in the powder bed but create a powder layer with a lower packing density [62]. However, the blade also has the side effect of a filtering mechanism for the bigger particles. The layer thickness affects the quality of the final piece, and its minimum value is equal to the diameter of the powder particles. Therefore, the dimension of the powder directly influences the quality of the powder bed. In fact, finer particles provide better packing densities that, as a consequence, reduce the risk of defect formation in as-built parts.

As discussed earlier, the particle size distribution of powders used for AM has a Gaussian distribution, and this trend, together with the processing parameters, can influence the melt pool stability. Nevertheless, this factor is not considered in the computational modelling that is performed to predict the thermomechanical interactions [45]. Therefore, this kind of modelling can be used for a generic part, and it is not so precise to be used to simulate the behaviour of special features like thin walls. Moreover, the capillary forces of the melt pool are another important factor that should be considered, especially when the melt pool dimension is in the powder size range. Therefore, if it is neglected in the simulation, a Plateau-Rayleigh instability will occur during the solidification of the track (Fig. 4) [63, 64]. This instability can cause the balling effect and result in very high surface roughness in the as-built part. However, it should be underlined that the influence of the process parameters on this instability is an easy task. However, it can be linked to the Volumetric energy density (VED, J/mm^3) that is delivered to a powder bed:

$$VED = \frac{nP}{v.t.d} \quad (2)$$

where VED is the volumetric energy density, n is the repeated scanning, P is the heat source power, v is the scanning speed, t is the layer thickness, and d is the hatching distance. It is reported that an excessive energy density can lead to a balling phenomenon due to the long presence of a liquid phase [54]. However, it is necessary to analyse also the effect of single parameters to comprehend the liquid–powder bed interaction in such a way that, for instance, the balling phenomenon can be avoided by using slower speeds and higher laser powers (keeping constant the VED).

In order to minimise the effects of the Plateau-Rayleigh instability and the inhomogeneity of the powder, the use of thinner layer thickness and slower scanning speed at a constant VED is recommended [64]. The other effects that should be considered in the process development are convection, the key-holes formation and evaporation in the melting pool [65]. In general, it is reported that the Gaussian distribution of the laser intensity and the motion of the heat source during the process results in a non-uniform temperature distribution within the melt pool [66]. Consequently, this temperature gradient leads to the formation of a flow in the melt pool, called "Marangoni convection" [67, 68]. As shown in Fig. 5, the temperature-surface tension gradients in the melt pool affect its shape and dimensions directly. The temperature will always be higher in the centre of the

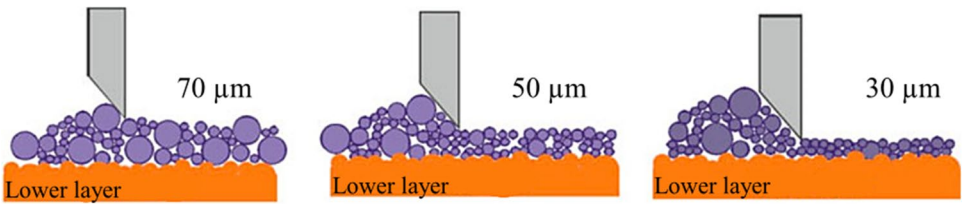

Fig. 3 Powder spread using a blade for different layer thicknesses [45]

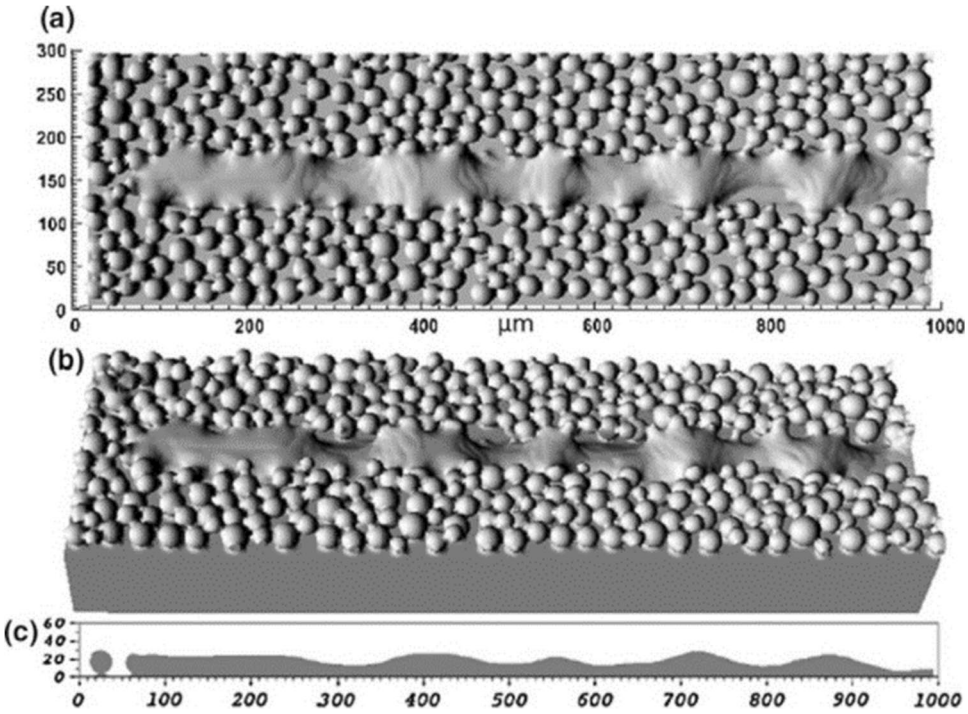

Fig. 4 Effects of the Plateau-Rayleigh instability on a single track: **a** *xy* plane; **b** instability of the single track melting; **c** depth of the melting pool [63]

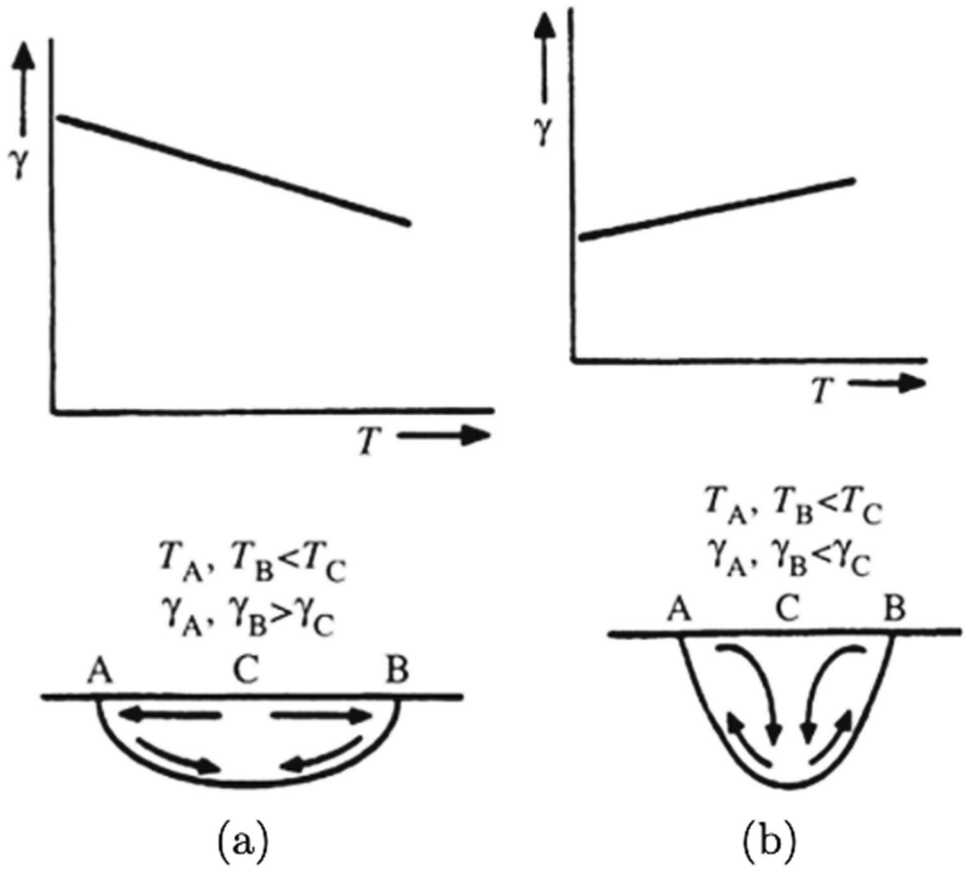

Fig. 5 Marangoni convection in the melting pool, the flow motion depends on the temperature-surface tension gradient: **a** negative temperature-surface tension gradient; **b** positive temperature-surface tension gradient [67]

melting pool due to the laser intensity distribution, so it is important to focus on the surface tension properties of the materials. If the surface tension is higher in the centre (Fig. 5b), the Marangoni flow tends to create a deeper melt pool and chemical homogeneity [69]. In contrast, there is a negative gradient for a surface tension higher at the melt pool boundaries (Fig. 5a), and the Marangoni flow creates a wider and flatter pool [67]. It is interesting to highlight that the Marangoni convection can sometimes be used as a turbulence effect to break the oxides on the surface of reactive materials like aluminium and titanium alloys [70]. On the other hand, the keyhole effect is strictly connected to the evaporation of alloying elements, particularly in a deep melt pool. In a deep melt pool, the gas cannot escape from the deepest part and is entrapped inside the melt pool, forming a vapour cavity defect [6]. Another aspect that should be considered is technical gas and its properties on the material used in the production. For instance, the lower thermal conductivity of argon compared to nitrogen can change the solidification rate and the defect formation and final density of the component [67, 71].

On the other hand, it is also well documented that the beam scanning strategy influences the thermal history of the piece, the distribution of thermal fields and temperature gradients [72]. Basically, a proper scanning strategy is a strategy that can simultaneously heat all the processed areas. It is very interesting to notice that in the EBM process, thanks to the higher speed of the heat source, it is possible to use a "multi-spot" strategy, in which different points are heated up very fast that could be assumed simultaneously. While for a laser process, due to some limitations in the beam deflection, the scanning speed is much slower than the EBM process, and as a result, this multi-beam concept is not available. As a consequence, the temperature distribution will have larger thermal gradients in the case of the laser-based process. Therefore several efforts have been undertaken to minimise this phenomenon and optimise the L-PBF process. One of the simplest solutions is using a proper scanning strategy by changing the vector length. In fact, using a shorter vector length would reduce the time to return and accordingly reheat the same point several times (Fig. 6) [73]. The shorter vector length helps reduce the residual thermal stress in the final part. Moreover, it is possible to change the vector direction layer by layer in order to reduce the anisotropy and the thermal distortion in the component. In fact, changing the vector direction can be performed in two ways (Fig. 7); the first one is the "alternate scanning," in which the direction of all the layers is rotated by 90° per layer, and

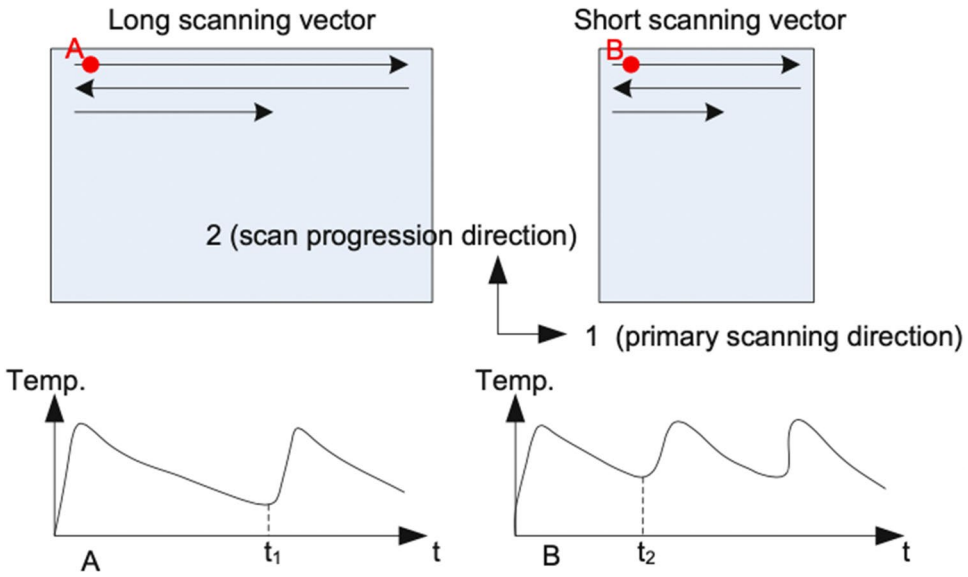

Fig. 6 Thermal history of two different scanning strategies with different vector lengths [6]

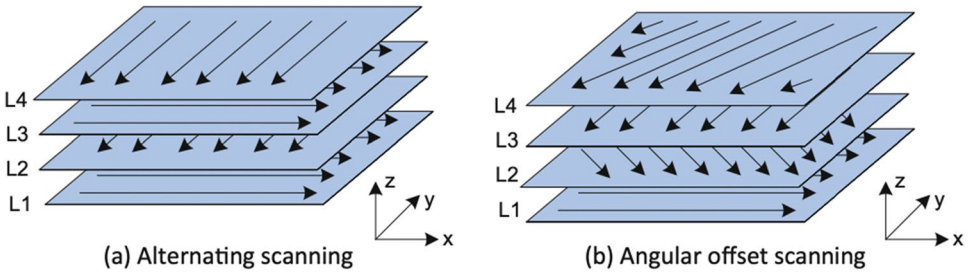

Fig. 7 Relationship between thermal gradient and the scanning vector length [10]

the second one is the "angular offset scanning," where the vectors are rotated by a fixed angle each layer [73].

Moreover, it is reported that an alternate scanning strategy can reduce around 30% of the thermal distortion with respect to a single direction scanning strategy. Analysing the residual stresses inside the single layer shows that the stress is generated in a direction perpendicular to the primary scanning direction [74].

In some cases, for complex geometries or design constraints, there are some limitations in the length of the scanning vector, so it is also possible to change the scanning strategy by dividing the layer into sub-regions to decrease the overall vector lengths. Since the stresses are perpendicular to the primary scanning direction, having sub-regions with different scanning directions can reduce the stress in the layer. However, this kind of scanning strategy results in a complex thermal history in the part that makes the study of temperature evolution in part very challenging. Considering both the thermal stress control and the operation perspectives, it is recommended to consider a good compromise using a moderate sub-region dimension. Another aspect must be considered is the sample orientation during the fabrication that influences the mechanical properties.

In general, several parameters, such as laser power, laser scanning speed, hatch distance, layer thickness, overhang angle, gas flow (speed and quantity), and scanning strategy, can affect the LPBF process [10]. However, the parameters that influence downskin quality are considered and explained in this overview. The first useful parameter to control the energy given in the melt pool is VED which is shown in Eq. 2. Among the involved parameters, the layer thickness is a parameter that can directly affect the quality of the part through the stair-stepping effect. Therefore, thinner layer thicknesses are recommended to minimise this effect and improve surface quality. As much as the layer is thinner, the production is more precise and has higher quality. However, this reduction in the layer thickness will negatively affect the production time and make the process less productive.

The laser power and laser scanning speed are usually defined according to a "process map" (Fig. 8), in which for low speeds and high powers, there can be a balling defect, or for low powers and high speeds, there would be a risk of defect formation. Therefore, it can be concluded that the central region where the combinations of process parameters give a high consolidation level should be considered the optimum process window [75]. On the other hand, hatching distance affects the porosity and the quality of the layer in such a way that by decreasing the hatching distance, the overlap between the melt pools would increase, and as a consequence, the risk of pore formation decreases. Like the layer thickness, the low hatching distances also negatively affected production time and made production less productive.

These kinds of process maps are very helpful in finding the optimised core parameters for simple geometries. However, in the case of complex geometries, such as thin walls, it should also be considered that the classic parameters are not enough to have a highly efficient production. In these cases, both combinations with the same power-to-speed ratio are recommended, but higher power and higher speed or lower power and lower speed (resulting in a finer resolution) [76].

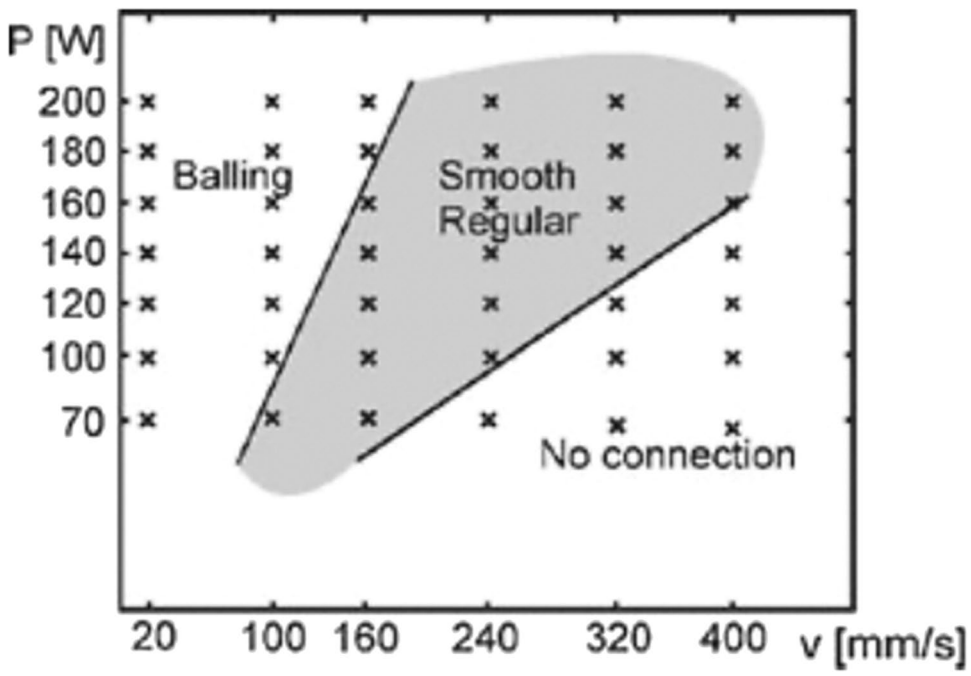

Fig. 8 Typical process map for L-PBF of a Fe – Ni – Cu – Fe_3P alloy [75]

As far as the overhanging surfaces are concerned, it is suggested to keep the energy density constant and decrease the power and speed or decrease the VED to decrease the amount of heat that has to be dissipated [75]. Another factor that can be used is the linear energy density (LED), which is the ratio between the power and speed of the laser:

$$\mathrm{LED} = \frac{\mathrm{P}}{\mathrm{v}} \tag{3}$$

4 Downskin parameters

Downskin is a term that indicates some layers (usually 1–4) above the supports or directly on the powder [77]. In general, downskin is usually considered as the three layers, and these should be processed using different parameters with respect to those of the "in-skin" or "core" ones [42]. As it is well documented, the heat conduction varies depending on the relative density. The heat conduction is one hundred times lower in powder layers with lower packing densities than in the solid-supported zone [36]. In fact, depending on their typology, the support structures can dissipate different heat levels, but on the other hand, the more it dissipates heat (e.g. block support), the more difficult it is to remove it [78, 79]. Several works have found that to obtain superior mechanical properties for the samples and surface finishing for the overhanging surfaces, it is recommended to use a solid/block support to dissipate more heat. Some representative of overhanging surfaces is shown in Fig. 9 [80].

However, this will also increase the cost in terms of material, time in the printing, and post-processing operations [80]. Apart from the heat dissipation, support structures are used to sustain the part and counterbalance the tensile forces during the rapid cooling of the melt pools, which can be a source of warping and delamination [42]. In the case of downward-facing surfaces, some shape and dimensional accuracy problems can occur if they are not well supported. Besides, an important factor is the inclined angle of an overhang surface, defined as the angle between the inclined surface and the horizontal plane. Depending on the materials and process parameters, there is a critical angle at which it would be possible to build the surfaces without using a support structure at angles higher than that critical one. However, this value does not assure good surface and mechanical properties [48]. Hence, it is very important to define a "reliable building angle" which is the minimum angle that can guarantee part production without dross formation and detachments [45]. Considering an industrial point of view, the possibility of creating overhanging surfaces without support by keeping a good quality (in terms of mechanical properties and surface finishing) is very important. Substantially, the parameters influencing the downskin quality are inclined angle, residual stress accumulation, VED, vector length on the overhanging surfaces fabrication and layer thickness (for the stair-stepping effect) [77]. The main problems in producing parts with overhanging surfaces without supports are warping, dross formation and staircase effect [48]. When the laser impacts the powder, it generates a melt pool whose dimensions depend on the VED and the heat conduction of the previous layers. Since the heat conduction for the powder is lower than that of bulk one, for the same VED, the melt pool in an overhanging surface without supports will be deeper and larger. Therefore, the melt pool can sink into the powder and cause dross formation on the downward-facing surface (Fig. 10) [80]. As a result, this dross formation leads to an increase in roughness and a low dimensional accuracy. On the other side, rapid solidification of the melt pool results in the warping phenomena [81]. In fact, when the generated stress is higher than the strength of the material, it causes a plastic deformation. Moreover, this effect will be magnified in the overhanging surfaces without supports due to the lack of solid support that can

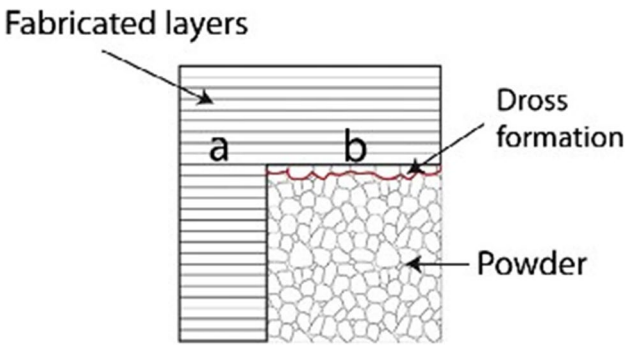

Fig. 10 A schematic of dross formation on a downward-facing surface [80]

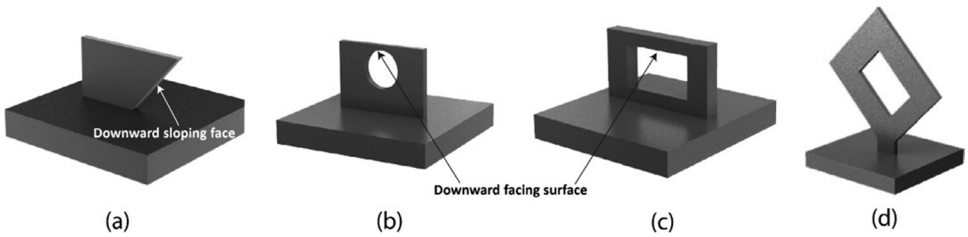

Fig. 9 Examples of overhanging surfaces: **a** downward sloping face, **b**, **c** downward-facing surfaces and **d** downward sloping faces [80]

counterbalance the tensile stresses [45]. When warping occurs, a localised increase of height in the boundary of the first layer with the warping will form and accumulate layers. In this situation, in the next layers, there will be less powder spread by the recoater. Consequently, the heat conduction decreases significantly, and the warping effect on the subsequent layers worsens [45].

After several layers, the created part will have lower mechanical resistance due to the presence of defects, and if the height of the warping effect exceeds the layer thickness (Fig. 11), the recoater blade can hit the layer, causing a detachment. The downskin, apart from the overhanging surfaces, is also important when building the horizontal holes (Fig. 12) [77].

A growing body of literature studied the correlation between the process parameters and the downskin quality [47, 77]. For instance, Bassoli et al. tried to figure out a generalised holistic method to test parameters for all the steps in fabricating a component through the LPBF process [47]. The horizontal layers above the support were considered the downskin surface in their work (Fig. 13). Their proposed method included a 3^3 factorial design (changing laser power, laser scanning speed and hatching distance), starting from a value of VED equal to 50% of the core one and increasing/decreasing by 20% ($VED_{downskin} = 50\% VED_{Core} \pm 20\%$). The suggested key performance indicators (KPI) were the absence of semidetached particles, cracks and sub-surface pores in the downskin surface. In general, in order to use this method, the knowledge of the effects of each parameter in the equation of VED would be requested. Indeed, the starting point of decreasing *VED* can make the idea, but there are infinite parameters and consequently different results for a fixed VED. Wang et al. reported the parameters affecting the quality of the overhang structure (Fig. 14) [45]. The laser power, laser scan speed, hatch distance, and layer thickness directly affect the VED and can vary, keeping a constant VED. Therefore, it is important to study the different effects of each parameter.

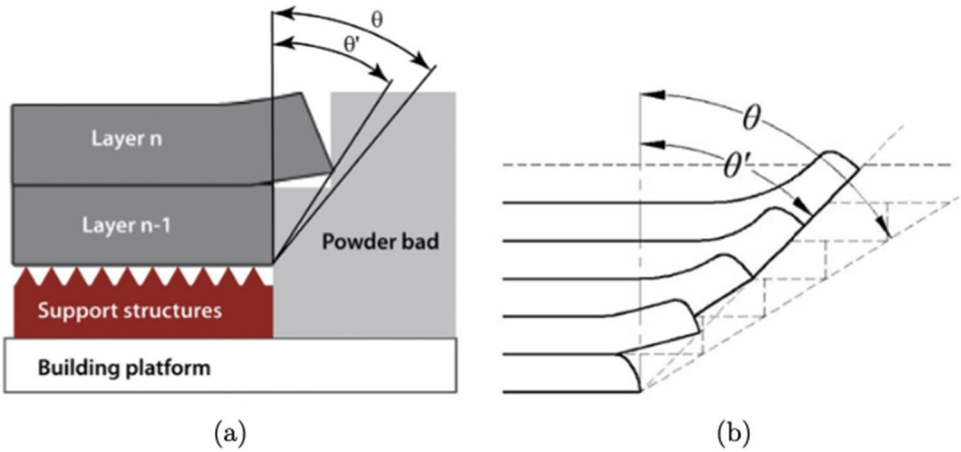

Fig. 11 Warping effects: **a** in a downward sloping face; **b** accumulation of warping effect [45]

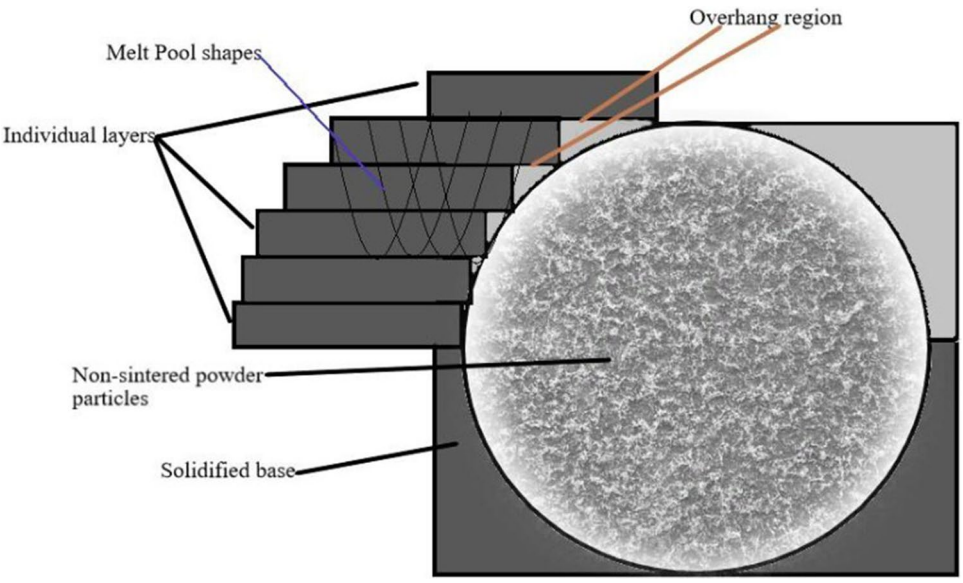

Fig. 12 Overhanging surfaces in a horizontal hole [77]

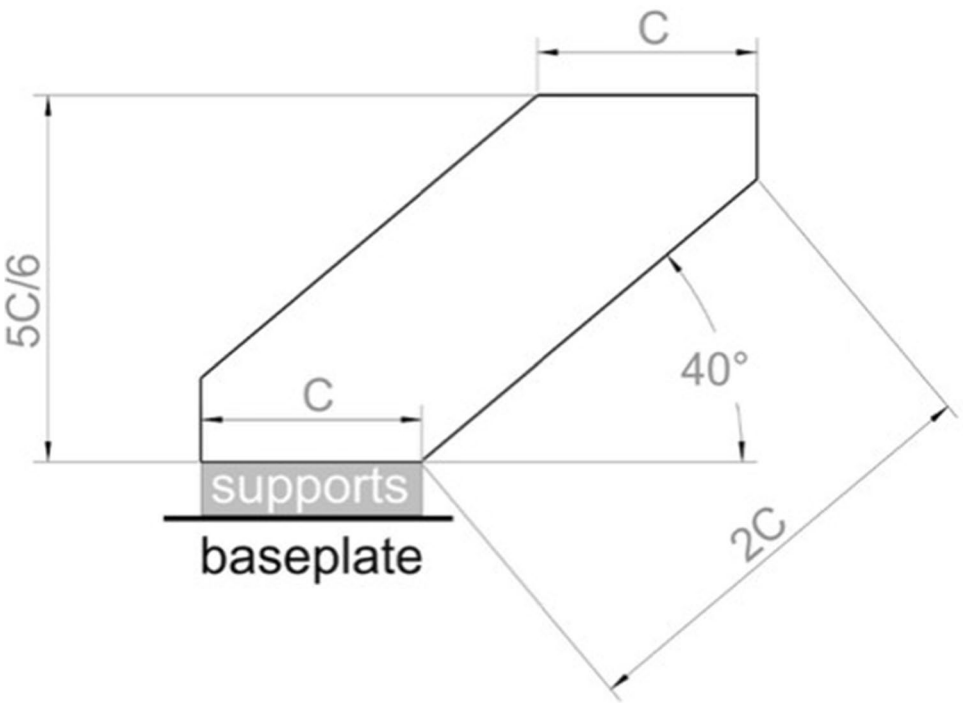

Fig. 13 The specimen used in the generalised method [47]

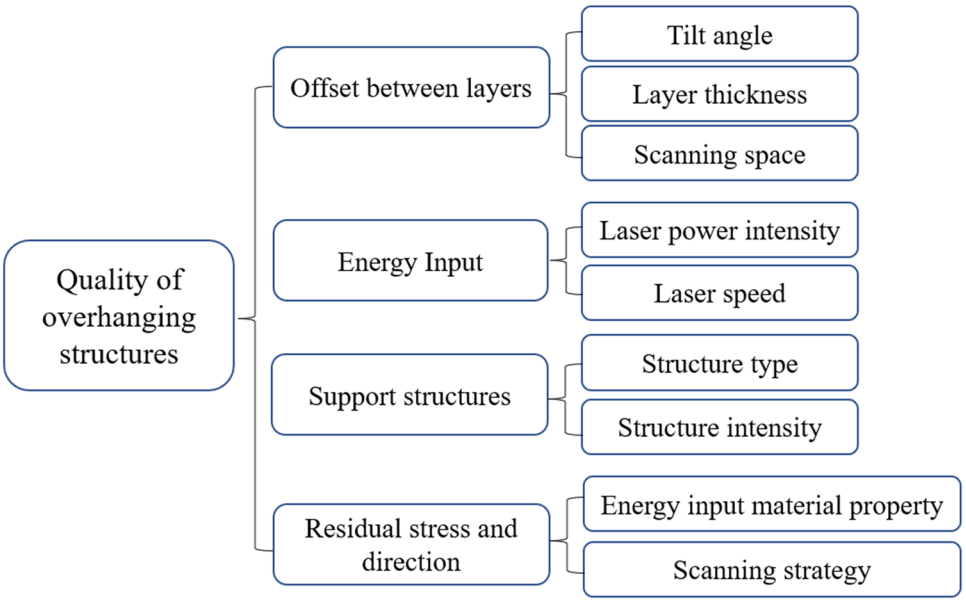

Fig. 14 Parameters affect the quality of an overhanging surface

4.1 Overhang angle

Downskin layers are considered both the layers used to build a horizontal surface above the supports, and the layers used to produce an oblique overhang surface. For the second case, the support structure is usually required for the overhang angles less than 45°. However, it should be highlighted that this specific minimum angle in which it can be built without support changes depends on the material ranging from 20° to 45° [82]. For instance, Wang et al. proposed a model to approximately evaluate the minimum building angle depending on layer thickness and overhanging length "S" between two adjacent layers (Fig. 15) [45].

The proposed equation is expressed as follows:

$$S = H \bullet \cot(\theta) \tag{4}$$

where H is the layer thickness, θ is the inclined angle, and S is the overhanging length between two adjacent layers. The smaller the angle for the same layer thickness, the smaller

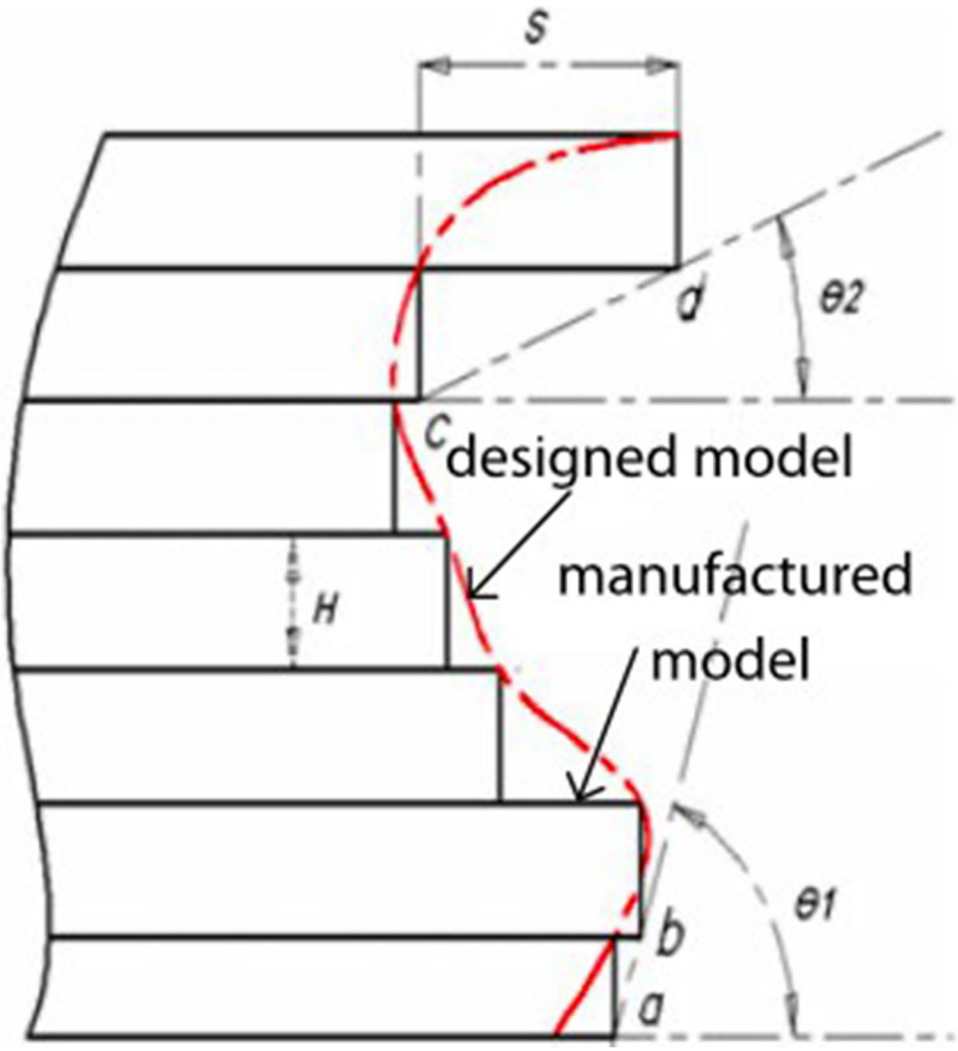

Fig. 15 Slicing model of a typical curved surface [45]

the tolerated overhanging length. However, there is a technical limitation in operation related to the laser spot size. As a matter of fact, the laser diameter used to focus on the solid-supported zone must be smaller than overhanging length S. Imposing this condition, it is possible to impose S equal to the laser spot, being able to evaluate the critical angle from Eq. 4. It is interesting to notice that their experimental results about the influence of the speeds confirm the outcomes of this equation. Sarkar et al. also employed this equation effectively in two experiments [50]. In fact, they succeeded in obtaining an unsupported specimen with an angle slightly smaller than that proposed by the calculation. It is important to notice that this minimum critical angle obtained by the equation does not predict any feature of mechanical properties. Wang et al. specified that by printing with a minimum angle calculated by this equation, the resulting downskin surface has a large dross formation and warping [45]. Other studies, like the one of Covarrubias and Eshraghi, revealed that by comparing two overhang oblique specimens built with an angle of 60° and 75°, the one with the smaller angle has more visible partially melted particles, causing an increase in roughness [48]. Basically, the effect of process parameters on the overhang angle should be analysed to obtain an unsupported oblique surface without dross formation and warping and with good mechanical characteristics to fulfil the production point of view. It is not critical to consider mechanical properties for the downskin layers in a horizontal surface above the support structure since there are just a few layers (1–4), and the vast majority of the part is built with core parameters [77]. Whereas, for the oblique overhanging surfaces, in which all the oblique parts of the component should be built with downskin parameters (if it is built without supports), it is necessary to study also the mechanical characteristics of the component [46, 83].

4.2 Power, speed and vector length

Besides the overhang angle, laser power, scanning speed and vector length are the other important parameters that affect the quality of the downskin surfaces. Therefore, over the

past years, several works have been carried out to study the effect of these parameters on the quality of the downward surfaces [45, 80]. As an example, Wang et al. analysed the influence of speed and power on the quality of the downward oblique surfaces of the AISI 316L specimens [45]. In their experiments, a Dimetal-280 system with maximum laser power and focused beam spot size of 200 W, and about 70 µm, respectively, were used. In their work, at first, the effect of scanning speed (200 to 1200 mm/s) and the overhang surface angle (50° to 25°) were investigated (Fig. 16). Thereafter, the effect of laser power in the range of 120 to 180 W on the quality of the overhang surface, particularly on dross formation and warping formation, was studied. Their outcomes proved the importance of inclined angle and scanning speed on fabrication quality. More in detail, they found that when the speed was 200 mm/s, the minimum building angle was slightly larger than 40°, while for a higher speed of 600 mm/s, the minimum building angle was above 30°. By increasing the velocity to 800 mm/s, the minimum building angle changed to a minimum value of 25°. Their findings were consistent with the concept that dross formation and warping effects are caused by higher input energy that cannot entirely be dissipated from the powder [84]. The drawback of using higher speeds, and consequently lower volume energy densities, is the high risk of defect formation, such as lack of fusion as a consequence of not enough input energy [85].

Moreover, they revealed that the real minimum angle was consistent with the outcomes of Eq. 1. In addition, it was found that by increasing the laser power when the other parameters were constant, the warping effect on the overhanging surface increased. For instance, when the power is 180 W, at a constant speed of 200 mm/s, the minimum building angle is 45° (higher than the one for 150 W). Interestingly, for speeds larger than 800 mm/s, the minimum angle was stable at 30° [45].

Furthermore, the effect of scanning vector length on the quality of the overhang surface was studied by Wang et al. [45]. Two symmetric parts of a sample with different vector lengths of 20 mm and 80 mm were produced in their work and analysed (Fig. 17). They found that in the case of using longer vectors, the warping was considerably more severe since there was more accumulation of internal stresses (Fig. 17), causing a break away from the supporting structure. These outcomes were consistent with the analysis results reported by Matsumoto et al. [86]. Matsumoto et al. proposed a method to calculate temperature and stress distribution within the solidified layer on the powder bed [86]. They also revealed that the warping is directly proportional to the vector length. In addition, it is reported that the solid

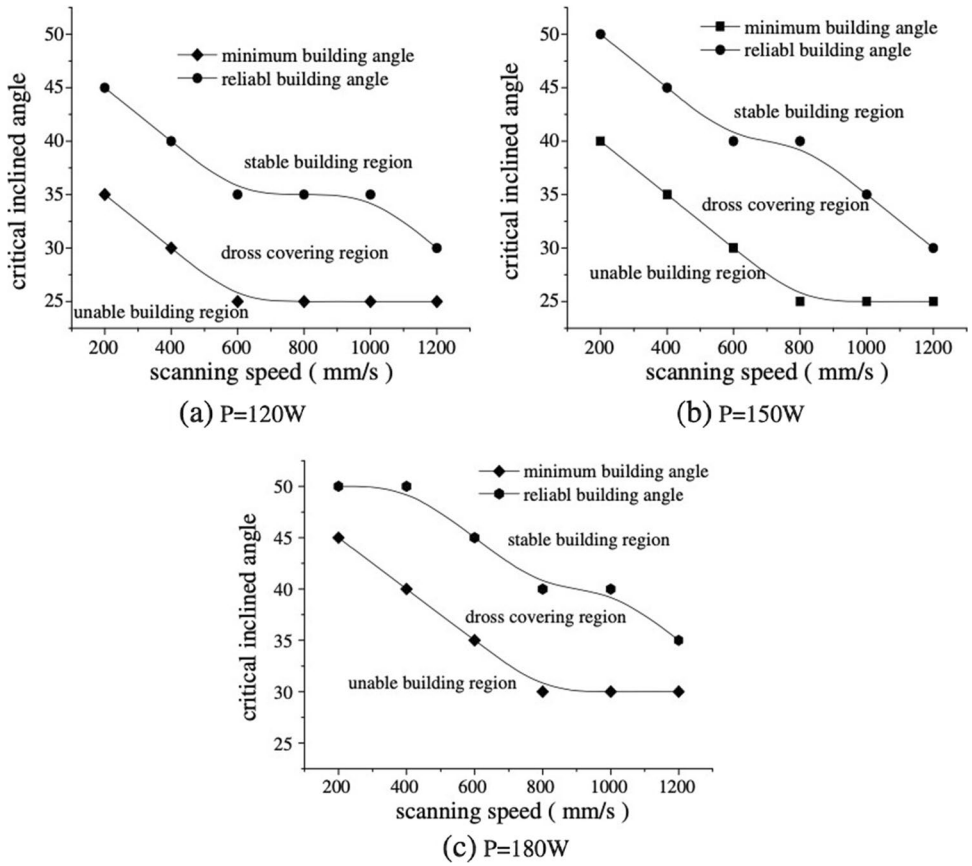

Fig. 16 Relationship between critical inclined angle and scanning speed at different laser power (scanning space 80 µm and layer thickness 35 µm). **a** $P = 120$ W, **b** $P = 150$ W, **c** $P = 180$ W [45]

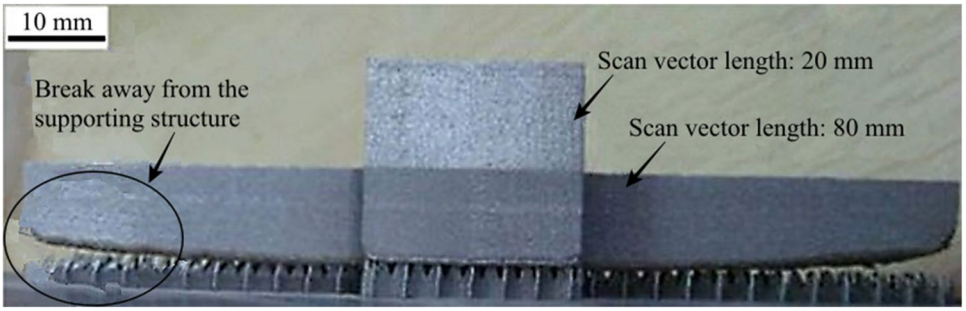

Fig. 17 Fabricating effect comparison for supported surfaces [45]

layer on the powder bed was warped owing to heating and cooling while the laser beam moved on the track. Considering an industrial point of view, a reliable angle to produce without using support structures is not enough because some specific mechanical characteristics and a maximum porosity allowed in part are also required. The same qualitative results, in terms of power and speed influences on the quality of the downskin surfaces, are also investigated by Calignano et al. [49].

4.3 Hatching distance

Apart from the laser-related parameters, hatching distance is also one of the main parameters that significantly influence the quality of the downskin surfaces. For instance, Calignano et al. studied the influence of process parameters on the porosity, accuracy and support structures of Hastelloy X produced via the L-PBF process [49]. For this reason, some cubes of $10 \times 10 \times 10$ mm^3 were produced using an EOSINT M270 Dual-mode system equipped with a Yb-fibre laser. The samples were produced using the same parameters for downskin, in-skin (or core) and up-skin. In fact, in their work, the effect of laser power (P), scanning speed (v) and hatching distance (h_d) at the constant stripe width (5 mm), the overlap of stripes (0.12 mm), layer thickness (20 µm), and contour parameters ($P = 150$ W and $v = 1250$ mm/s) were analysed. Firstly, they analysed the specimens and found the optimised set of parameters. The second step was to optimise the parameters to reduce the detachment of the downskin layers from the supports. They highlighted that the optimisation problem for the first layers above the support structure is the difference in released energy in the downskin layers (due to the parameters' variation from support to part production). Consequently, this discrepancy causes variations in the melt pool size and temperature, increasing the risk of deformations and detachments from the support structures (Fig. 18). Indeed, the role of support to dissipate the heat from the melting pool is important to decrease the thermal stresses and counterbalance the force of the recoating blade, which can create a dynamic pressure against the leading edge of the layer. The values used for the tests regarding the downskin values are reported in Table 1.

Table 2 presents three process parameters and their corresponding volume (Eq. 3) and linear (Eq. 4) energy density that was used by Calignano et al. [49]. However, it should be noticed that the support parameters are already optimised for Hastelloy X to avoid detachment between preheated plate and support. The interface between the support structure and downskin layers for all the samples listed in Table 2 is shown in Fig. 19. As can be seen, the best result was the one obtained for sample 6, while all the other specimens have balling problems with consequent delamination due to the blade impact. In that work, the support structure was a block type, shown in Fig. 19b, made of thin walls and powder. In this case, the heat conduction of the support is lower than the bulk material. For this reason, to avoid dross formation on the downskin surface, it is recommended to have less heat to be dissipated in the melt pools. Interestingly, sample 6 had

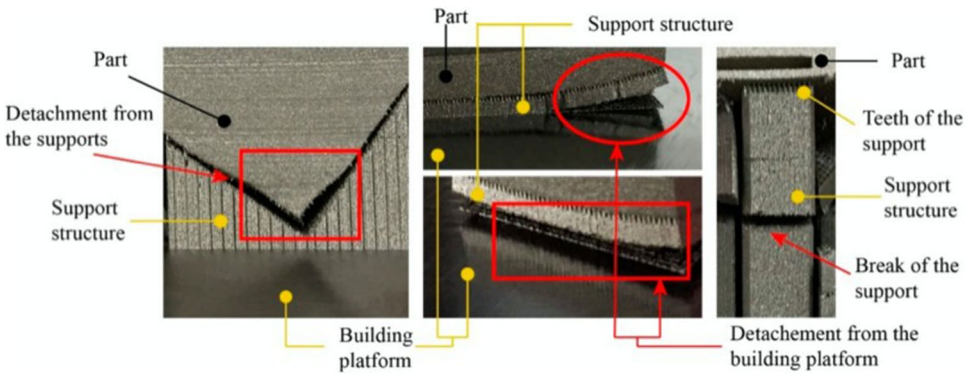

Fig. 18 The detachment between support and part (left), detachments of the support from the building platform (centre), and breaking of the support (right) in manufacturing for Inconel 718 [49]

Table 1 Process parameters, volume energy density and linear energy density for downskin and support [49]

	Sample	P [W]	v [mm/s]	H_d [mm]	VED [J/mm^3]	LED [J/mm]
Downskin (2 layers)	1	195	1000	0.05	195.00	0.195
	2	170	1000	0.05	170.00	0.170
	3	195	1000	0.08	121.88	0.195
	4	195	870	0.08	140.09	0.224
	5	170	870	0.08	122.13	0.195
	6	170	1000	0.08	106.25	0.170
	7	170	870	0.05	195.40	0.195
	8	195	870	0.05	224.14	0.224
Supports	–	80	400	–	–	0.200

Table 2 Parameters that have been reported for Hastelloy®X [87]

S. no	Skin power [W]	Scan rate [mm/s]	Hatch [µm]	Pre-sinter P [W]	Pre-sinter v [mm/s]	Pre-sinter hatch [µm]
1	370	1300	190			
2	370	1300	190	180	900	130
3	340	1150	210			
4	340	1150	210	180	900	130
5	360	1000	210			
6	360	1000	210	180	900	130
7	300	1000	190			
8	370	1600	190			
9	370	2000	210			
10	340	2000	210			

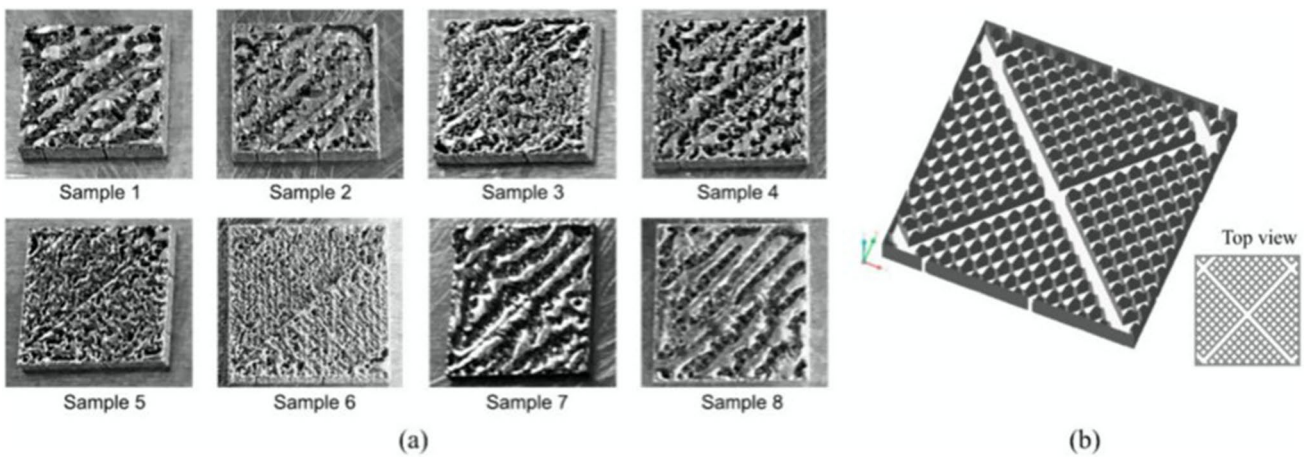

Fig. 19 **a** The interface between the support structure and downskin layer; **b** support structure of block type [49]

the lowest VED, consistent with the idea that recommended lower energies for the downskin layers. However, analysing the results obtained in terms of linear energy density is more interesting. Considering this aspect, it was found that both sample 2 and sample 6 have the lowest LE, but the downskin quality was different (Fig. 19a). This difference confirms the importance of the hatching distance on the quality of the downskin. This finding has also been reported by Bertoli et al. [88] and by Calignano et al. [89]. The dependence of the VED on the hatching distance is inversely proportional in such a way that the higher the h_d, the lower the VED, and consequently, the best results are obtained using the higher

value of hatching distance. Nevertheless, it should be highlighted that the mechanical properties of the core part are independent of the downskin parameters (Table 2). Therefore, it can be concluded that the choice of parameters for the support and downskin layers is very important to avoid large internal stresses and delaminations.

4.4 Scanning strategy and aspect ratio

Scanning strategy and aspect ratio are the other parameters that can play important roles in the quality of the downskin surfaces. Sarkar et al. studied the quality of overhang oblique surfaces without supports [50]. They compared the effects of the scanning strategy in terms of the angle and the "aspect ratio" (Fig. 20a). They evaluated the minimum critical angle using the same equation (Eq. 4) proposed by Wang et al. [90]. They found that the critical angle for stainless steel PH1 produced via the LPBF process using the layer thickness of 20 μm and the laser beam radius of 40 μm is 26.6°. Their founding is completely consistent with the works by Wang et al. [45], and Calignano et al. [49, 80]. It can be concluded that there is a consequent decrease in the overhang length when the angle decreases. If it is smaller than the beam diameter, there will be a consequent dross formation. Moreover, the overhang surface is unsupported, and since the powder has heat conduction lower than the bulk material, the dimensions of the melt pool become larger, resulting in dross formation. The values of the parameter "*a*" used are 2.5 (ratio 1:2), 3.5 (ratio 3.5:5) and 5 (ratio 1:1), and it is possible to see in Fig. 21 the results. At a fixed angle of 25°, they found that by increasing the ratio, there will be a worsening in warping and dross formation as a direct consequence of the larger contact area between the lower overhang oblique surface and unmelted powder. Practically a larger contact area will cause a decrease in heat conduction, and then warping will occur.

Thereafter, the effect of the scanning strategy, using fixed parameters, was analysed in three specimens with angles of 25°, 30° and 35° using a linear scanning strategy (Fig. 22a) and an alternate scanning strategy (Fig. 22b). In terms of energy density, using a linear scanning strategy, there is the same scanning direction for every layer. This will cause an increase in energy density so that the overhanging edges get repetitively heated up in the same regions. Changing the scanning strategy into an alternate one resulted in a decrease in energy density. The results were found to be in good agreement with the theoretical explanation. In fact, the degree of warping and the dross formation are qualitatively

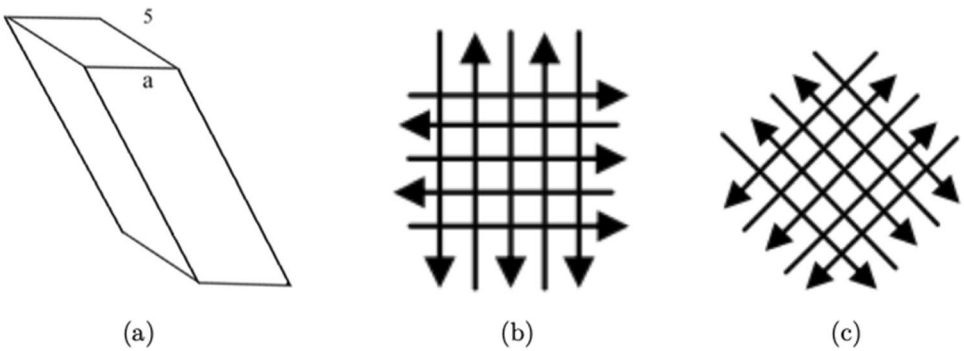

Fig. 20 Experiment: **a** specimen used, the aspect ratio is *a*: 5, with *a* = 5, 3.5, 2.5; **b** linear scan strategy; **c** alternate scan strategy [50]

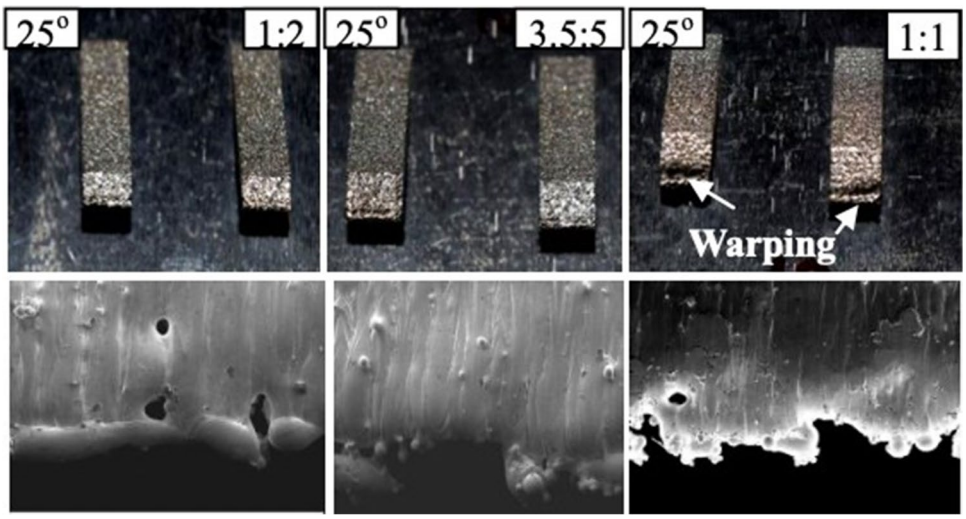

Fig. 21 Specimens obtained with different aspect ratios (above) and SEM images(below)

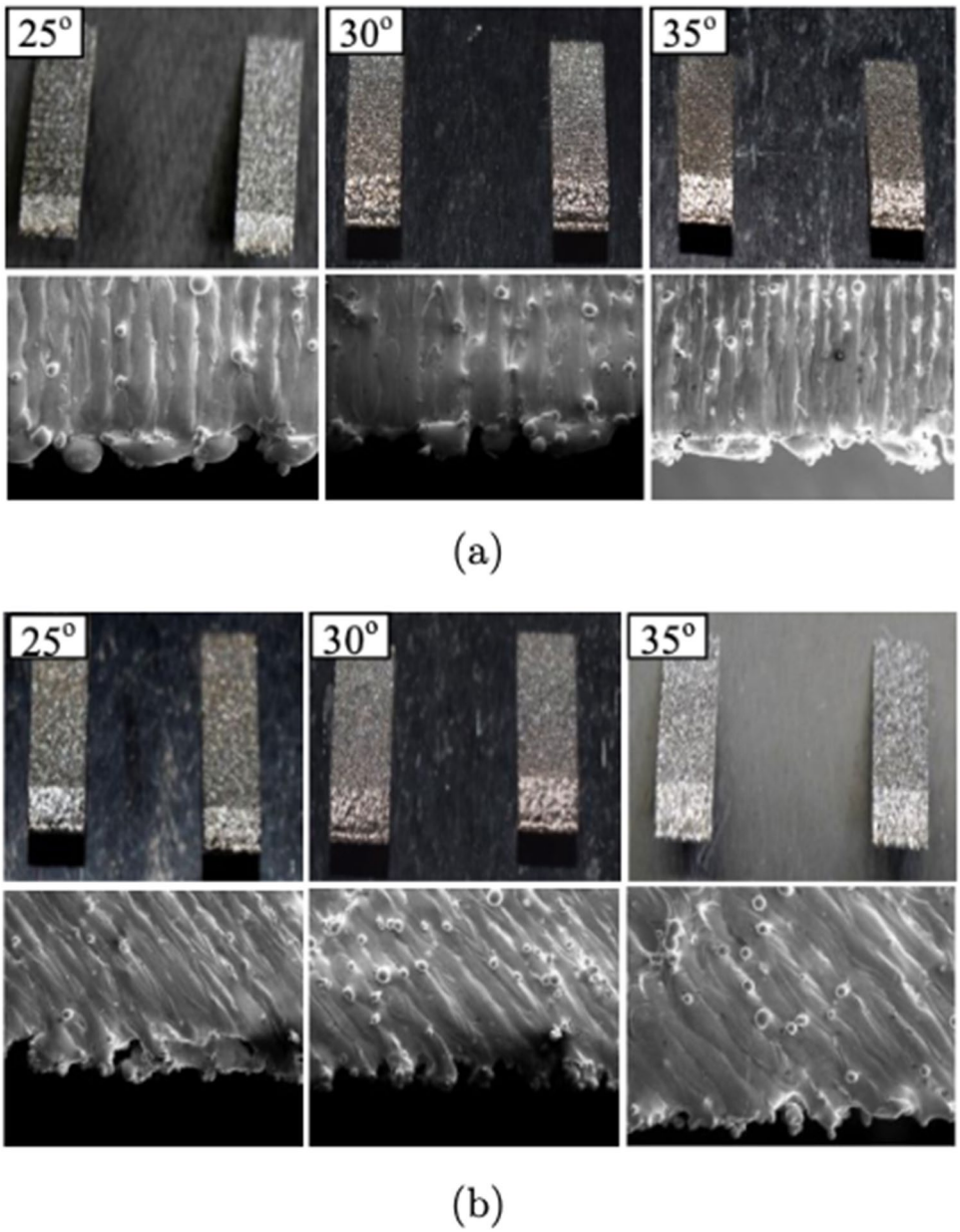

Fig. 22 Experiment: **a** linear scanning strategy; **b** alternate scanning strategy

decreased using a lower energy density. The minimum angle obtained in this experiment was 25.3°, lower than the theoretical one obtained from Eq. 4 (26.6°). What is lacking in these experiments is a quantitative analysis of the specimens. As a matter of fact, it is possible to produce components with downskin surfaces with an angle of 25.3°, but their mechanical properties were not evaluated.

4.5 Number of layers and pre-sintering

As the last important parameters, the number of layers and pre-sintering have been considered and studied over the past years. For instance, Khan et al. studied the influence of the number of layers printed with downskin parameters above a horizontal hole (Fig. 12) [77]. The upper half of the horizontal hole can be seen as an inclined overhang with a continuous decrement of the angle. For this reason, cubes of $5 \times 5 \times 5$ mm^3 of AlSi10Mg were produced using the fixed layer thickness of 30 µm, spot size diameter of 100 µm and the scanning strategy, alternate at 67°. Their work studied the effect of different processing parameters such as laser power, scan speed, hatching distance and finally, the number of downskin layers for core layers (Table 3). The parameters used for the downskin and upskin layers are those provided by EOS and have been kept constant: $P_{downskin} = 360$ W, $v_{downskin} = 1000$ mm/s, $P_{upskin} = 340$ W, $v_{upskin} = 1150$ mm/s. A small hole with a diameter of 0.5 mm is placed in the centre of the cube.

Table 3 Parameters used in the second experiment to optimise the downskin parameter for Hastelloy®X alloy [87]

S. no	Laser power [W]	Scan rate [mm/s]	Layers
1	65	1000	3
2	65	1000	4
3	65	1000	5
4	65	1000	6
5	150	1000	3
6	150	1000	4
7	150	1000	5

The influence of a pre-sintering strategy on the quality of the hole was also investigated.

In the case of the horizontal hole, the dross formation was revealed for the upper half, in which the high VED combined with low heat conduction due to the powder below the downskin layers caused a large and deep melt pool. It is very interesting to point out that a lower dross formation was found in the case of samples using pre-sintering. Figure 23 shows the outcomes of an ANSYS analysis for the depth of the melt pool in the first layer. As can be seen, both sets of parameters formed a melt pool deeper than the layer thickness, which will also melt the powder below the layer. This uncontrolled melting was found to be the reason for dross formation.

Khan et al. also simulated the depth of the melt pool using different parameters and compared the differences between the powder and solidly supported melt pools [77]. Their results in Fig. 24 clearly showed that the solid-supported layers have melt pools with a depth lower than the powder-supported ones. The SEM analysis of the horizontal hole quality demonstrated that all the holes are characterised by heavy dross formation (Fig. 25). It is possible to conclude that the pre-sintering does not affect the quality of the hole, and also, it is not possible to avoid dross formation with the parameters used in Table 3.

After that, the influence of the number of layers printed with downskin parameters, which is a fundamental constraint for the quality of overhanging surfaces, was investigated. For this reason, the effect of changing this number of layers into 4, 5 and 6 was considered and studied. Increasing the distance between the powder below the downskin and the

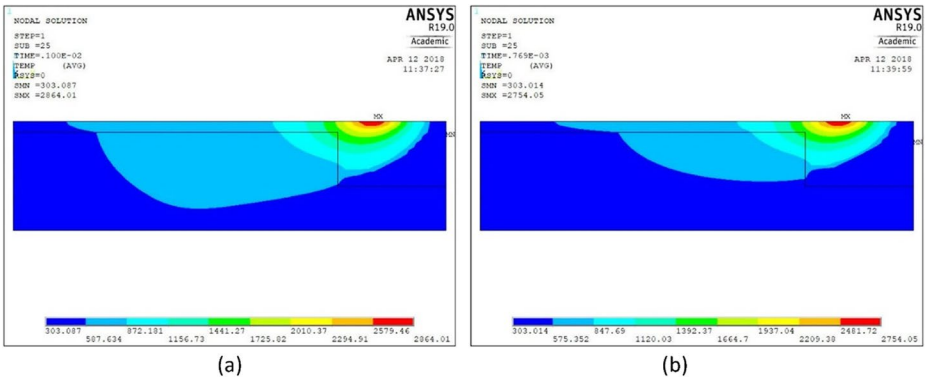

Fig. 23 Temperature distribution and melt pools: **a** downskin parameters $P = 360$ W, $v = 1000$ mm/s; **b** core parameters $P = 370$ W, $v = 1300$ mm/s [77]

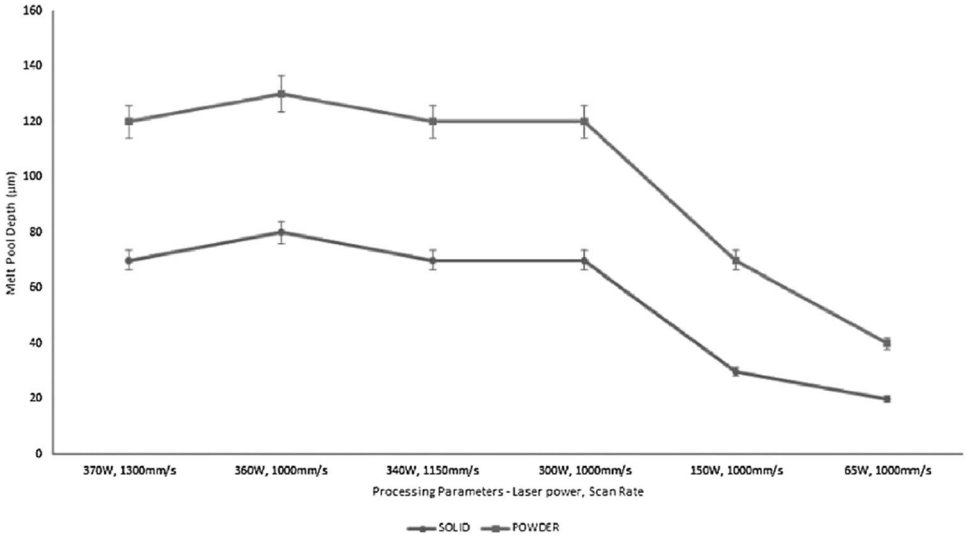

Fig. 24 Melt pool depth for different parameters. The upper line represents the values obtained for the powder supported layers, while the bottom line identifies the solid-supported layers [77]

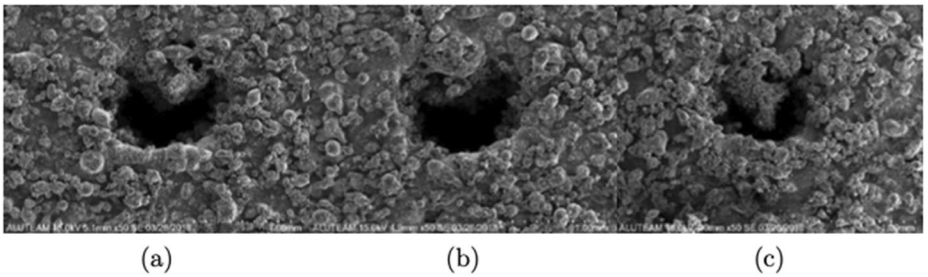

Fig. 25 SEM images for some specimens in Table 2: **a** specimen 1; **b** specimen 3; **c** specimen 6 [77]

first core layer (characterised by higher VED and a deeper melt pool) should be possible to decrease or avoid the dross formation. In fact, if the depth of the melt pool with core parameters is smaller than the height of all the layers printed with downskin parameters, the dross formation should be avoided. The parameters used to study the effect of the number of layers on the downskin quality are reported in Table 3.

Figure 26 compares the quality of the holes in different samples. As can be seen in this figure, by changing the parameters with respect to the ones in Table 3 (varying the number of layers printed in downskin parameters and the laser power), the results are always better in terms of dross formation compared to the previous ones (Fig. 25). Indeed, the holes in Fig. 26 have a circumference more precise than the ones in Fig. 25, due to less dross formation.

Among all the specimens, the best ones were numbers 2, 3 and 4, which show a small dross formation. These specimens have lower laser powers and several processed layers with downskin parameters higher than 3. Khan et al. also provided the ANSYS analysis for these two powers (65 and 150 W), and the results are presented in Fig. 27 [77]. This analysis clearly showed that the depth of the melt pools is lower with respect to those of the first experiment in the first downskin layer. For the layers above the first one, the heat prefers to escape to the previously solidified layer that has higher heat conduction rather than going to the less conductive region of the powder [38, 91].

Finally, Khan et al. used numerical analysis to study the effect of the first layer printed in core parameters [77]. The numerical analysis is made when the first layer with core parameters is printed after three downskin layers (Fig. 28). Indeed, it is important to study the depth of the first layer, which must not pass through all the downskin layers or will cause dross formation. It is possible to observe that the depth of the pool is larger than three layers, causing dross formation. This evidence is consistent with the SEM images analysed previously in which, by increasing the number of layers processed with downskin parameters from 3 to 4, the dross formation is decreased. However, from Fig. 26, it is also possible to see that when the number of layers printed with downskin parameters (65 W) increased, the region printed with downskin parameters had a higher porosity content due to insufficient liquid penetration.

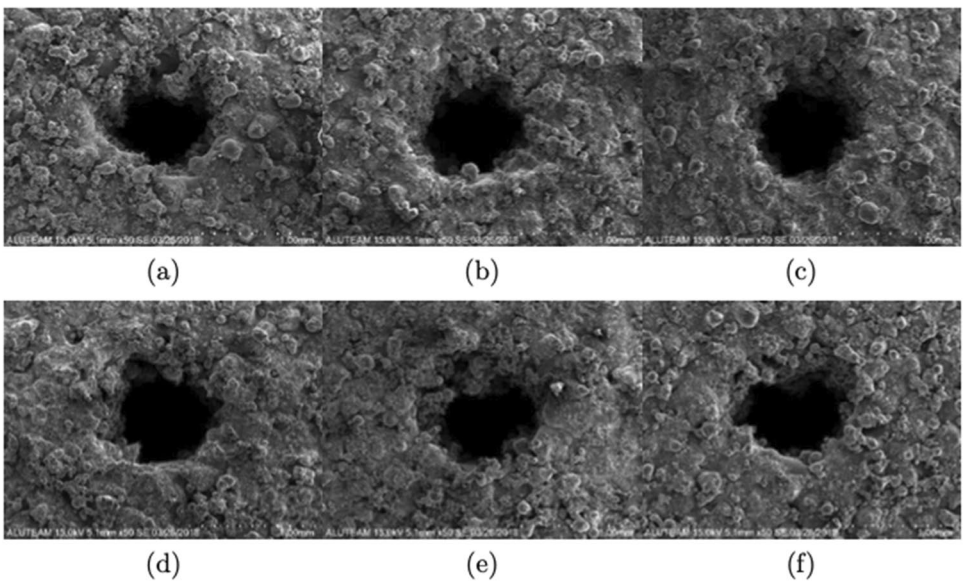

Fig. 26 SEM images for some specimens in Table 3: **a** specimen 1; **b** specimen 2; **c** specimen 3; **d** specimen 4; **e** specimen 5; **f** specimen 6 [77]

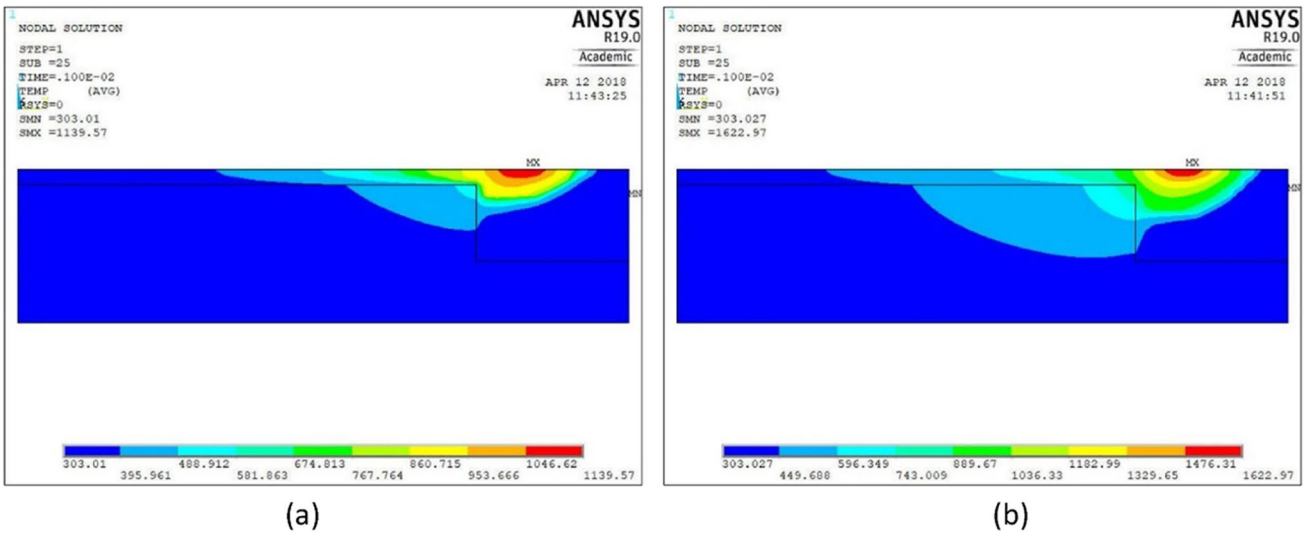

Fig. 27 Temperature distribution at **a** $P = 65$ W and $v = 1000$ m/s; **b** $P = 150$ W and $v = 1000$ mm/s [77]

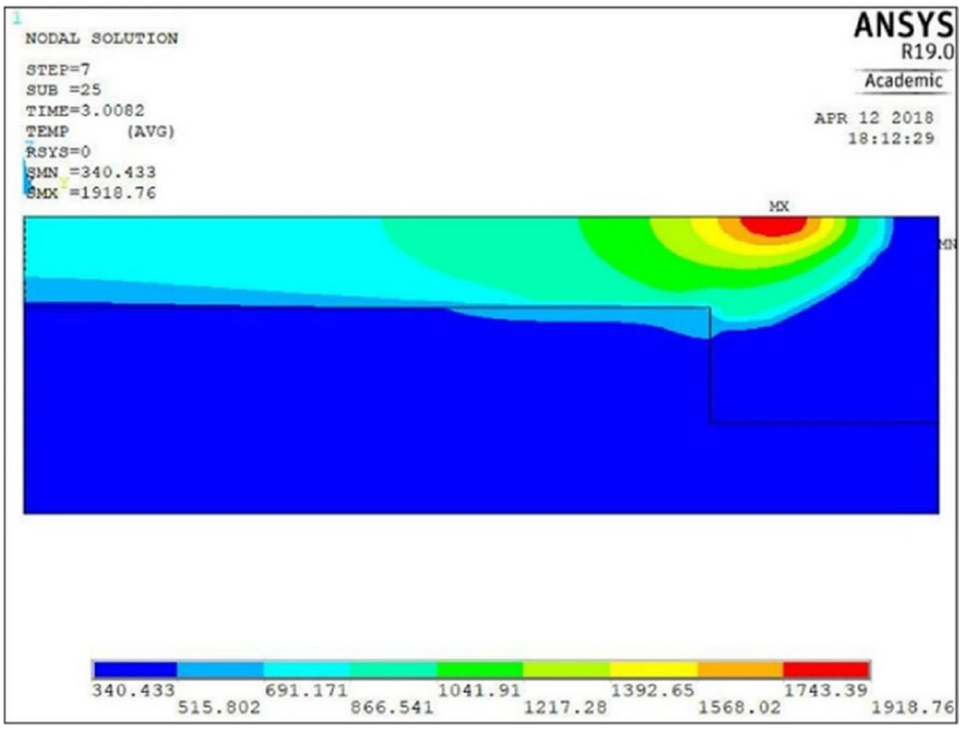

Fig. 28 Temperature distribution for the 4th layer printed with core parameters (360 W, 1000 mm/s) after three layers using downskin parameters (65 W, 1000 mm/s) [77]

5 Future perspective

Over the past years, metal AM could attract much attention in academia and industry. Thus, this paper focuses on the latest progress in the state of the art regarding optimising downskin process parameters that are different from those of the hatch one. In general, finding the optimum process parameters for producing complex shape components using metal AM processes is one of the first critical steps. In this phase, finding the best parameters for the downskin surfaces is crucial and should be implemented beside the standard optimisation of process parameters. So far, several efforts have been undertaken to tune the process parameters related to the downward surfaces and enhance their surface quality in the as-built state. For this reason, all the effective parameters, such as the overhang angle,

laser power, laser scanning speed, scanning strategy, etc., have been identified and evaluated in detail.

Nevertheless, all these efforts are materials and geometric related in such a way that a new optimisation is required to be considered by slightly changing the chemical composition or geometry. Therefore, in the next step of technology development, this aspect might be considered important and provide a standard procedure for each class of material. Implementation of this general procedure can result in obtaining an enhanced surface quality for overhang surfaces in the as-built state. As a consequence of this improvement, lew support structures will be required, and as a result, the lead time would be shortened, and cost would decrease markedly. In addition, the authors strongly believe that microscale simulations on the melt-pool involvement in the downskin area can predict and direct the optimisation of the parameters avoiding costly trials and tests.

6 Conclusion

In this work, a comprehensive overview has been performed on the effects of processing parameters on the quality of the downskin surfaces. According to the key finding on these subjects, the following conclusions can be drawn as follows:

- Theoretical studies showed a minimum printable angle (critical angle) for each alloy to be processed via the L-PBF process. These studies demonstrate that large dross formation and warping characterises the overhang printed with angles below the critical angle.
- The experimental works showed that through optimisation of process parameters, it would be possible to print the overhangs with a specific angle without dross formation and defects.
- Dross formation and warping are caused by higher energy input: printing an overhang with a smaller angle for lower power is possible using a constant speed.
- Warping was directly proportional to the vector length.
- Hatch distance influences the quality of the piece related to the creation of internal stresses and delamination.
- The scanning strategy and the aspect ratio play an important role in the quality of the overhang surfaces.
- An alternate scanning reduces the delamination according to the reduction of volume energy density with respect to the linear scanning strategy.
- Increasing the number of layers printed with the downskin parameters to 4–6 downskin layers reduces the dross formation since the melt pool of the first core layer does not pass through all the downskin region, avoiding dross.

Author contribution V.V and J.S collect the manuscript for the literature, analyse the papers and wrote the first draft of the paper, A.S, F.B and A.S verified the data analyses, supervise and review and edit the manuscript.

Funding Open access funding provided by Politecnico di Torino within the CRUI-CARE Agreement.

Data availability The datasets generated during and/or analysed during the current study are available from the corresponding author on reasonable request.

Code availability Not applicable.

Declarations

Ethics approval This chapter does not contain any studies with human participants or animals performed by any of the authors. Authors acknowledge the work is original and all the relevant text from the literature has been properly cited.

Consent to participate Authors agree to the authorship order.

Consent for publication All authors have read and agreed to the published version of the manuscript.

Conflict of interest The authors declare no competing interests.

References

1. Oliveira JP, LaLonde AD, Ma J (2020) Processing parameters in laser powder bed fusion metal additive manufacturing. Mater Des 193:1–12. https://doi.org/10.1016/j.matdes.2020.108762
2. Behjat A, Shamanian M, Taherizadeh A, Noori M, Lannunziata E, Iuliano L, Saboori A (2022) Enhanced surface properties and bioactivity of additively manufactured 316L stainless steel using different post-treatments. Mater Today Proc. https://doi.org/10.1016/j.matpr.2022.09.019
3. Saboori A, Gallo D, Biamino S, Fino P, Lombardi M (2017) An overview of additive manufacturing of titanium components by directed energy deposition: Microstructure and mechanical properties. Appl Sci 7:883. https://doi.org/10.3390/app7090883
4. Dadkhah M, Saboori A, Fino P (2019) An overview of the recent developments in metal matrix nanocomposites reinforced by graphene. Materials (Basel) 12:2823. https://doi.org/10.3390/ma12172823
5. Ghorbani HR, Mosallanejad MH, Atapour M, Galati M, Saboori A (2022) Hybrid additive manufacturing of an electron beam powder bed fused Ti6Al4V by transient liquid phase bonding. J Mater Res Technol 20:180–194. https://doi.org/10.1016/j.jmrt.2022.07.009

6. Yang L, Hsu K, Baughman B, Godfrey D, Medina F, Menon M, Wiener S (2017) Additive manufacturing of metals: the technology, materials, design and production. https://doi.org/10.1007/978-3-319-55128-9.
7. Maleki E, Bagherifard S, Bandini M, Guagliano M (2021) Surface post-treatments for metal additive manufacturing: progress, challenges, and opportunities. Addit Manuf 37:101619. https://doi.org/10.1016/J.ADDMA.2020.101619
8. Aversa A, Saboori A, Marchese G, Iuliano L, Lombardi M, Fino P (2021) Recent progress in beam-based metal additive manufacturing from a materials perspective: a review of patents. J Mater Eng Perform 30:8689–8699. https://doi.org/10.1007/s11665-021-06273-3
9. Saboori A, Aversa A, Bosio F, Bassini E, Librera E, De Chirico M, Biamino S, Ugues D, Fino P, Lombardi M (2019) An investigation on the effect of powder recycling on the microstructure and mechanical properties of AISI 316L produced by Directed Energy Deposition. Mater Sci Eng A 766:138360. https://doi.org/10.1016/j.msea.2019.138360
10. Milewski JO (2017) Springer series in materials science 258 additive manufacturing of metals. https://doi.org/10.1007/978-3-319-58205-4.
11. Kumar N, Bhavsar H, Mahesh PVS, Srivastava AK, Bora BJ, Saxena A, Dixit AR (2022) Wire arc additive manufacturing – a revolutionary method in additive manufacturing. Mater Chem Phys 285:126144. https://doi.org/10.1016/j.matchemphys.2022.126144
12. Ramalho A, Santos TG, Bevans B, Smoqi Z, Rao P, Oliveira JP (2022) Effect of contaminations on the acoustic emissions during wire and arc additive manufacturing of 316L stainless steel. Addit Manuf 51:102585. https://doi.org/10.1016/j.addma.2021.102585
13. Ke WC, Oliveira JP, Cong BQ, Ao SS, Qi ZW, Peng B, Zeng Z (2022) Multi-layer deposition mechanism in ultra high-frequency pulsed wire arc additive manufacturing (WAAM) of NiTi shape memory alloys. Addit Manuf 50:102513. https://doi.org/10.1016/j.addma.2021.102513
14. ISO/ASTM International (2021) Additive manufacturing — general principles — fundamentals and vocabulary. In: ISO/ASTM 52900:2021, ASTM International, West Conshohocken (USA), Volume 12/17/2021
15. Mosallanejad MH, Niroumand B, Ghibaudo C, Biamino S, Salmi A, Fino P, Saboori A (2022) In-situ alloying of a fine grained fully equiaxed Ti-based alloy via electron beam powder bed fusion additive manufacturing process. Addit Manuf 56:102878. https://doi.org/10.1016/j.addma.2022.102878
16. Nedjad SH, Yildiz M, Saboori A (2022) Solidification behaviour of austenitic stainless steels during welding and directed energy deposition. Sci Technol Weld Join 1–17. https://doi.org/10.1080/13621718.2022.2115664
17. Saboori A, Piscopo G, Lai M, Salmi A, Biamino S (2020) An investigation on the effect of deposition pattern on the microstructure, mechanical properties and residual stress of 316L produced by Directed Energy Deposition. Mater Sci Eng A 780:139179. https://doi.org/10.1016/j.msea.2020.139179
18. Davoodi E, Montazerian H, Mirhakimi AS, Zhianmanesh M, Ibhadode O, Shahabad SI, Esmaeilizadeh R, Sarikhani E, Toorandaz S, Sarabi SA, Nasiri R, Zhu Y, Kadkhodapour J, Li B, Khademhosseini A, Toyserkani E (2022) Additively manufactured metallic biomaterials. Bioact Mater 15:214–249. https://doi.org/10.1016/j.bioactmat.2021.12.027
19. Souflas T, Bikas H, Ghassempouri M, Salmi A, Atzeni E, Saboori A, Brugnetti I, Valente A, Mazzucato F, Stavropoulos P (2022) A comparative study of dry and cryogenic milling for Directed Energy Deposited IN718 components: effect on process and part quality. Int J Adv Manuf Technol 119:745–758. https://doi.org/10.1007/s00170-021-08313-7
20. Griffiths ER, Leigh SJ (2022) Hybrid additive manufacture: surface finishing methods for improving conductivity of inkjet printed tracks on non-planar substrates fabricated using fused deposition modeling. Sensors Actuators A Phys 333:113235. https://doi.org/10.1016/j.sna.2021.113235
21. Zhang J, Lee YJ, Wang H (2021) A brief review on the enhancement of surface finish for metal additive manufacturing. J Miner Metal Mater Eng 7:1–14
22. Nagalingam AP, Yeo SH (2020) Surface finishing of additively manufactured Inconel 625 complex internal channels: a case study using a multi-jet hydrodynamic approach. Addit Manuf 36:101428. https://doi.org/10.1016/j.addma.2020.101428
23. Galati M, Defanti S, Saboori A, Rizza G, Tognoli E, Vincenzi N, Gatto A, Iuliano L (2022) An investigation on the processing conditions of Ti-6Al-2Sn-4Zr-2Mo by electron beam powder bed fusion: Microstructure, defect distribution, mechanical properties and dimensional accuracy. Addit Manuf 50:102564. https://doi.org/10.1016/j.addma.2021.102564
24. Saboori A, Biamino S, Lombardi M, Tusacciu S, Busatto M, Lai M, Fino P (2019) How the nozzle position affects the geometry of the melt pool in directed energy deposition process. Powder Metall 62:213–217. https://doi.org/10.1080/00325899.2019.1627490
25 Wohlers TT, Campbell I, Diegel O, Huff R, Kowen J (2021) Wohlers Associates: Wohlers report 2021: 3D printing and additive manufacturing global state of the industry. Wohlers Assoc, Fort Collins
26. Körner C, Attar E, Heinl P (2011) Mesoscopic simulation of selective beam melting processes. J Mater Process Technol 211:978–987. https://doi.org/10.1016/J.JMATPROTEC.2010.12.016
27. Gong X, Anderson T, Chou K (2014) Review on powder-based electron beam additive manufacturing technology. Manuf Rev 1:2
28. Leal R, Barreiros FM, Alves L, Romeiro F, Vasco JC, Santos M, Marto C (2017) Additive manufacturing tooling for the automotive industry. Int J Adv Manuf Technol 92:1671–1676. https://doi.org/10.1007/s00170-017-0239-8
29. Del Guercio G, Galati M, Saboori A (2021) Electron beam melting of Ti-6Al-4V lattice structures: correlation between post heat treatment and mechanical properties. Int J Adv Manuf Technol 116:3535–3547. https://doi.org/10.1007/s00170-021-07619-w
30. de Formanoir C, Suard M, Dendievel R, Martin G, Godet S (2016) Improving the mechanical efficiency of electron beam melted titanium lattice structures by chemical etching. Addit Manuf 11:71–76
31. Wauthle R, Vrancken B, Beynaerts B, Jorissen K, Schrooten J, Kruth J-P, Van Humbeeck J (2015) Effects of build orientation and heat treatment on the microstructure and mechanical properties of selective laser melted Ti6Al4V lattice structures. Addit Manuf 5:77–84. https://doi.org/10.1016/j.addma.2014.12.008
32. Cansizoglu O, Harrysson O, Cormier D, West H, Mahale T (2008) Properties of Ti–6Al–4V non-stochastic lattice structures fabricated via electron beam melting. Mater Sci Eng A 492:468–474
33. Thole KA, Lynch SP, Wildgoose AJ (2021) Chapter Five - Review of advances in convective heat transfer developed through additive manufacturing. In: Abraham JP, Gorman JM, Minkowycz W (eds) Elsevier, pp. 249–325. https://doi.org/10.1016/bs.aiht.2021.06.004.
34. Ashby A, Guss G, Ganeriwala RK, Martin AA, DePond PJ, Deane DJ, Matthews MJ, Druzgalski CL (2022) Thermal history and high-speed optical imaging of overhang structures during laser powder bed fusion: A computational and experimental analysis. Addit Manuf 53:102669. https://doi.org/10.1016/j.addma.2022.102669
35. Kasperovich G, Becker R, Artzt K, Barriobero-Vila P, Requena G, Haubrich J (2021) The effect of build direction and geometric optimization in laser powder bed fusion of Inconel 718 structures

with internal channels. Mater Des 207:109858. https://doi.org/10.1016/j.matdes.2021.109858
36. Wang D, Yang Y, Zhang M, Lu J, Liu R, Xiao D (2013) Study on SLM fabrication of precision metal parts with overhanging structures. IEEE International Symposium on Assembly and Manufacturing (ISAM), pp 222–225. https://doi.org/10.1109/ISAM.2013.6643532
37 Jiang J, Xu X, Stringer J (2018) Support structures for additive manufacturing: a review. J Manuf Mater Process 2:64. https://doi.org/10.3390/jmmp2040064
38. Oter ZC, Coskun M, Akca Y, Surmen O, Yilmaz MS, Ozer G, Tarakci G, Khan HM, Koc E (2019) Support optimization for overhanging parts in direct metal laser sintering. Optik (Stuttg) 181:575–581. https://doi.org/10.1016/j.ijleo.2018.12.072
39. Gan MX, Wong CH (2016) Practical support structures for selective laser melting. J Mater Process Technol 238:474–484. https://doi.org/10.1016/j.jmatprotec.2016.08.006
40. Charles A, Elkaseer A, Thijs L, Hagenmeyer V, Scholz S (2019) Effect of process parameters on the generated surface roughness of down-facing surfaces in selective laser melting. Appl Sci 9:1256. https://doi.org/10.3390/app9061256
41. Spierings AB, Herres N, Levy GN (2010) Influence of the particle size distribution on surface quality and mechanical properties in additive manufactured stainless steel parts. In: Proc. Solid Free. Fabr. Symp. Austin, TX, USA
42. Vayre B, Vignat F, Villeneuve F (2012) Designing for additive manufacturing. Procedia CIRP 3:632–637. https://doi.org/10.1016/j.procir.2012.07.108
43. Atzeni E, Salmi A (2015) Study on unsupported overhangs of AlSi10Mg parts processed by Direct Metal Laser Sintering (DMLS). J Manuf Process 20:500–506
44. Salmi A, Calignano F, Galati M, Atzeni E (2018) An integrated design methodology for components produced by laser powder bed fusion (L-PBF) process. Virtual Phys Prototyp 13:191–202
45. Wang D, Yang Y, Yi Z, Su X (2013) Research on the fabricating quality optimization of the overhanging surface in SLM process. Int J Adv Manuf Technol 65:1471–1484. https://doi.org/10.1007/s00170-012-4271-4
46. Cabanettes F, Joubert A, Chardon G, Dumas V, Rech J, Grosjean C, Dimkovski Z (2018) Topography of as built surfaces generated in metal additive manufacturing: a multi scale analysis from form to roughness. Precis Eng 52:249–265. https://doi.org/10.1016/j.precisioneng.2018.01.002
47 Bassoli E, Sola A, Celesti M, Calcagnile S, Cavallini C (2018) Development of laser-based powder bed fusion process parameters and scanning strategy for new metal alloy grades: A holistic method formulation. Materials (Basel). 11:2356. https://doi.org/10.3390/ma11122356
48. Covarrubias EE, Eshraghi M (2018) Effect of build angle on surface properties of nickel superalloys processed by selective laser melting. Jom 70:336–342. https://doi.org/10.1007/s11837-017-2706-y
49. Calignano F, Minetola P (2019) Influence of process parameters on the porosity, accuracy, roughness, and support structures of hastelloy X produced by laser powder bed fusion. Materials (Basel) 12:1–10. https://doi.org/10.3390/ma12193178
50. Sarkar S, Porwal A, Yaswanth N, Nath AK (2018) A study on effect of different process parameters on the quality of overhang surface produced by selective laser melting, ASME 2018 13th Int. Manuf Sci Eng Conf MSEC 2018(1):1–7. https://doi.org/10.1115/MSEC2018-6421
51 Mosallanejad MH, Niroumand B, Aversa A, Manfredi D, Saboori A (2020) Laser Powder Bed Fusion in-situ alloying of Ti-5%Cu alloy: process-structure relationships. J. Alloys Compd 857:157558. https://doi.org/10.1016/j.jallcom.2020.157558
52. Aristizabal M, Jamshidi P, Saboori A, Cox SC, Attallah MM (2020) Laser powder bed fusion of a Zr-alloy: Tensile properties and biocompatibility. Mater Lett 259:126897. https://doi.org/10.1016/j.matlet.2019.126897
53. Mosallanejad MH, Niroumand B, Aversa A, Saboori A (2021) In-situ alloying in laser-based additive manufacturing processes: a critical review. J Alloys Compd 872:159567. https://doi.org/10.1016/j.jallcom.2021.159567
54. Aversa A, Marchese G, Saboori A, Bassini E, Manfredi D, Biamino S, Ugues D, Fino P, Lombardi M (2019) New aluminum alloys specifically designed for laser powder bed fusion: a review. Materials (Basel) 12:1007
55. Yadroitsev I, Krakhmalev P, Yadroitsava I (2017) Titanium alloys manufactured by in situ alloying during laser powder bed fusion. JOM 69:2725–2730. https://doi.org/10.1007/s11837-017-2600-7
56. DebRoy T, Wei HL, Zuback JS, Mukherjee T, Elmer JW, Milewski JO, Beese AM, Wilson-Heid A, De A, Zhang W (2018) Additive manufacturing of metallic components – process, structure and properties. Prog Mater Sci 92:112–224. https://doi.org/10.1016/j.pmatsci.2017.10.001
57. Mosallanejad MH, Sanaei S, Atapour M, Niroumand B, Iuliano L, Saboori A (2022) Microstructure and corrosion properties of CP-Ti processed by laser powder bed fusion under similar energy densities. Acta Metall Sin (English Lett) 35:1453–1464. https://doi.org/10.1007/s40195-022-01376-9
58. Strano G, Hao L, Everson RM, Evans KE (2013) A new approach to the design and optimisation of support structures in additive manufacturing, Int J Adv Manuf Technol 66:1247–1254. https://doi.org/10.1007/s00170-012-4403-x
59. Saboori A, Abdi A, Fatemi SA, Marchese G, Biamino S, Mirzadeh H (2020) Hot deformation behavior and flow stress modeling of Ti–6Al–4V alloy produced via electron beam melting additive manufacturing technology in single β-phase field. Mater Sci Eng A 792:139822. https://doi.org/10.1016/j.msea.2020.139822
60 Del Guercio G, Galati M, Saboori A, Fino P, Iuliano L (2020) Microstructure and mechanical performance of Ti–6Al–4V lattice structures manufactured via electron beam melting (EBM): a review. Acta Metall Sin (Engl Lett). 33:183–203. https://doi.org/10.1007/s40195-020-00998-1
61. Sochalski-Kolbus LM, Payzant EA, Cornwell PA, Watkins TR, Babu SS, Dehoff RR, Lorenz M, Ovchinnikova O, Duty C (2015) Comparison of residual stresses in Inconel 718 simple parts made by electron beam melting and direct laser metal sintering. Metall Mater Trans A Phys Metall Mater Sci 46:1419–1432. https://doi.org/10.1007/s11661-014-2722-2
62. Zheng M, Wei L, Chen J, Zhang Q, Zhong C, Lin X, Huang W (2019) A novel method for the molten pool and porosity formation modelling in selective laser melting. Int J Heat Mass Transf 140:1091–1105
63. King W, Anderson AT, Ferencz RM, Hodge NE, Kamath C, Khairallah SA (2015) Overview of modelling and simulation of metal powder bed fusion process at Lawrence Livermore National Laboratory. Mater Sci Technol 31:957–968. https://doi.org/10.1179/1743284714Y.0000000728
64. Körner C, Bauereiß A, Attar E (2013) Fundamental consolidation mechanisms during selective beam melting of powders. Model Simul Mater Sci Eng 21:085011. https://doi.org/10.1088/0965-0393/21/8/085011
65. Panwisawas C, Qiu CL, Sovani Y, Brooks JW, Attallah MM, Basoalto HC (2015) On the role of thermal fluid dynamics into the evolution of porosity during selective laser melting. Scr Mater 105:14–17
66. Mirkoohi E, Ning J, Bocchini P, Fergani O, Chiang K-N, Liang SY (2018) Thermal modeling of temperature distribution in metal additive manufacturing considering effects of build layers, latent

heat, and temperature-sensitivity of material properties. J Manuf Mater Process 2:63
67 Hondros ED, McLean M, Mills KC, Mills KC, Keene BJ, Brooks RF, Shirali A (1998) Marangoni effects in welding. Philosophical Transactions of the Royal Society of London. Ser A Math Phys Eng Sci 356:911–925
68. Mills KC, Keene BJ, Brooks RF, Shirali A (1998) Marangoni effects in welding. Philos Trans R 356:911–925. https://doi.org/10.1098/rsta.1998.0196
69. Li B, Wang L, Wang B, Li D, Oliveira JP, Cui R, Yu J, Luo L, Chen R, Su Y, Guo J, Fu H (2022) Electron beam freeform fabrication of NiTi shape memory alloys: Crystallography, martensitic transformation, and functional response. Mater Sci Eng A 843:143135. https://doi.org/10.1016/j.msea.2022.143135
70. Olakanmi EO, Cochrane RF, Dalgarno KW (2015) A review on selective laser sintering/melting (SLS/SLM) of aluminium alloy powders: processing, microstructure, and properties. Prog Mater Sci 74:401–477. https://doi.org/10.1016/j.pmatsci.2015.03.002
71. Aversa A, Saboori A, Librera E, de Chirico M, Biamino S, Lombardi M, Fino P (2020) The role of directed energy deposition atmosphere mode on the microstructure and mechanical properties of 316L samples. Addit Manuf 34:101274. https://doi.org/10.1016/j.addma.2020.101274
72. Ni C, Zhu L, Zheng Z, Zhang J, Yang Y, Hong R, Bai Y, Lu WF, Wang H (2020) Effects of machining surface and laser beam scanning strategy on machinability of selective laser melted Ti6Al4V alloy in milling. Mater Des 194:108880
73 Li C, Liu JF, Fang XY, Guo YB (2017) Efficient predictive model of part distortion and residual stress in selective laser melting. Addit Manuf 17:157–168
74. Neugebauer F, Keller N, Ploshikhin V, Feuerhahn F, Köhler H (2014) Multi scale FEM simulation for distortion calculation in additive manufacturing of hardening stainless steel. International Workshop on Thermal Forming and Welding Distortion, Bremen
75. Kruth JP, Froyen L, Van Vaerenbergh J, Mercelis P, Rombouts M, Lauwers B (2004) Selective laser melting of iron-based powder. J Mater Process Technol 149(1–3):616–622
76. Yadroitsev I, Bertrand P, Smurov I (2007) Parametric analysis of the selective laser melting process. Appl Surf Sci 253:8064–8069. https://doi.org/10.1016/j.apsusc.2007.02.088
77. Khan HM, Dirikolu MH, Koç E (2018) Parameters optimization for horizontally built circular profiles: Numerical and experimental investigation. Optik (Stuttg) 174:521–529. https://doi.org/10.1016/j.ijleo.2018.08.095
78. Mirzendehdel AM, Suresh K (2016) Support structure constrained topology optimization for additive manufacturing. Comput Des 81:1–13
79. Gao W, Zhang Y, Ramanujan D, Ramani K, Chen Y, Williams CB, Wang CCL, Shin YC, Zhang S, Zavattieri PD (2015) The status, challenges, and future of additive manufacturing in engineering. Comput Des 69:65–89. https://doi.org/10.1016/j.cad.2015.04.001
80. Calignano F (2014) Design optimization of supports for overhanging structures in aluminum and titanium alloys by selective laser melting. Mater Des 64:203–213. https://doi.org/10.1016/j.matdes.2014.07.043
81. Le KQ, Wong CH, Chua KHG, Tang C, Du H (2020) Discontinuity of overhanging melt track in selective laser melting process. Int J Heat Mass Transf 162:120284
82. Leary M, Merli L, Torti F, Mazur M, Brandt M (2014) Optimal topology for additive manufacture: a method for enabling additive manufacture of support-free optimal structures. Mater Des 63:678–690
83. Allaire G, Dapogny C, Estevez R, Faure A, Michailidis G (2017) Structural optimization under overhang constraints imposed by additive manufacturing technologies. J Comput Phys 351:295–328
84. Shange M, Yadroitsava I, du Plessis A, Yadroitsev I (n.d.) Roughness and near-surface porosity of unsupported overhangs produced by high-speed laser powder bed fusion, 3D print. Addit Manuf 0 null. https://doi.org/10.1089/3dp.2020.0097
85 RoccettiCampagnoli M, Galati M, Saboori A (2021) On the processability of copper components via powder-based additive manufacturing processes: potentials, challenges and feasible solutions. J Manuf Process 72:320–337. https://doi.org/10.1016/j.jmapro.2021.10.038
86. Matsumoto M, Shiomi M, Osakada K, Abe F (2002) Finite element analysis of single layer forming on metallic powder bed in rapid prototyping by selective laser processing. Int J Mach Tools Manuf 42(1):61–67
87. Bertoli US, Wolfer AJ, Matthews MJ, Delplanque JPR, Schoenung JM (2017) On the limitations of Volumetric Energy Density as a design parameter for Selective Laser Melting. Mater Des 113:331–340
88. Bertoli US, Matthews MJ, Wolfer AJ, Matthews MJ, Delplanque J-PR, Schoenung JM (2016) On the limitations of Volumetric Energy Density as a design parameter for Selective Laser Melting Laser-matter interactions and Laser damage science View project Hydrogen Storage Program at LLNL View project On the limitations of Volumetric Energy Density. Elsevier. https://doi.org/10.1016/j.matdes.2016.10.037.
89. Calignano F, Cattano G (n.d.) D.M.-J. of M. Processing, undefined 2018, Manufacturing of thin wall structures in AlSi10Mg alloy by laser powder bed fusion through process parameters. Elsevier. https://www.sciencedirect.com/science/article/pii/S092401361830030X
90. Wang X, Deng D, Qi M, Zhang H (2016) Influences of deposition strategies and oblique angle on properties of AISI316L stainless steel oblique thin-walled part by direct laser fabrication. Opt Laser Technol 80:138–144. https://doi.org/10.1016/j.optlastec.2016.01.002
91. Farshidianfar MH, Khajepour A, Gerlich AP (2016) Effect of real-time cooling rate on microstructure in laser additive manufacturing. J Mater Process Technol 231:468–478. https://doi.org/10.1016/j.jmatprotec.2016.01.017